1-1-2011

Dual-Fueling Concepts: a Comparison of Methane and Propane as Primary Fuels with Biodiesel and Ultra-Low Sulfur Diesel as Separate Pilot Fuels

Nicholas Thane Shoemaker

DUAL-FUELING CONCEPTS: A COMPARISON OF METHANE AND PROPANE AS PRIMARY FUELS WITH BIODIESEL AND ULTRA-LOW SULFUR DIESEL AS SEPARATE PILOT FUELS

By

Nicholas Thane Shoemaker

A Thesis
Submitted to the Faculty of
Mississippi State University
in Partial Fulfillment of the Requirements
for the Degree of Master of Science
in Mechanical Engineering
in the Department of Mechanical Engineering

Mississippi State, Mississippi

December 2011

DUAL-FUELING CONCEPTS: A COMPARISON OF METHANE AND PROPANE AS PRIMARY FUELS WITH BIODIESEL AND ULTRA-LOW SULFUR DIESEL AS SEPARATE PILOT FUELS

By

Nicholas Thane Shoemaker

Approved:

Kalyan K. Srinivasan Assistant Professor of Mechanical Engineering (Director of Thesis)	Sundar R. Krishnan Assistant Professor of Mechanical Engineering (Co-Major Professor/Committee Member)
Pedro Mago Associate Professor of Mechanical Engineering (Committee Member)	Steven R. Daniewicz Professor and Department Head of Mechanical Engineering (Graduate Coordinator)

Sarah A. Rajala
Dean of the Bagley College of Engineering

Name: Nicholas Thane Shoemaker

Date of Degree: December 9, 2011

Institution: Mississippi State University

Major Field: Mechanical Engineering

Major Professor: Dr. Kalyan K. Srinivasan

Title of Study: DUAL-FUELING CONCEPTS: A COMPARISON OF METHANE AND PROPANE AS PRIMARY FUELS WITH BIODIESEL AND ULTRA-LOW SULFUR DIESEL AS SEPARATE PILOT FUELS

Pages in Study: 58

Candidate for Degree of Master of Science

The goal of this thesis is to examine dual-fueling concepts using two different types of primary fuel, methane and propane; as well as two different pilot fuels, ultra-low sulfur diesel (ULSD) and biodiesel (B100). Experiments were performed using a 1.9 liter, turbocharged, 4 cylinder diesel engine at 1800 rev/min with ULSD and B100 being injected as a pilot fuel directly into the combustion chamber, at different brake mean effective pressures (BMEP), and percent energy substitutions of propane and methane. Brake thermal efficiency (BTE) and emissions (NO_x, THC, CO, CO_2, O_2 and smoke) were also measured and analyzed. Maximum PES was limited by misfire at 2.5 bar, 5.0 bar, 7.5 bar, BMEP for all cases and knock at 10 bar BMEP for both B100-propane and ULSD-propane. In general dual fueling was shown to be beneficial for lowering NO_x, CO_2, and smoke emissions along with, in some cases, showing improvements in BTE.

DEDICATION

Dedicated to my Lord and Savior Jesus Christ; my wife, Shawna, whose patience and support has been unending, and to my daughter, Ellie.

ACKNOWLEDGEMENTS

I would like to thank my advisors Dr. Kalyan Srinivasan and Dr. Sundar Krishnan whose support, guidance, and instruction has been imperative to my research and professional growth. I would also like to thank my friends and colleagues, Michael Gibson and Andrew Polk, whose collaboration has been undeniably important in this research. Additional thanks is due to my other committee member Dr. Pedro Mago for his assistance and support.

I would also like to acknowledge the financial support of the Sustainable Energy Research Center (US DOE Award # DE-FG36-06GO86025) and facilities support from the Center for Advanced Vehicular Systems at Mississippi State University.

TABLE OF CONTENTS

DEDICATION ii

ACKNOWLEDGEMENTS iii

LIST OF TABLES vi

LIST OF FIGURES vii

NOMENCLATURE ix

CHAPTER

I. INTRODUCTION 1

II. EXPERIMENTAL SETUP 5

III. DUAL-FUEL INVESTIGATIONS: BIODIESEL PILOT FUEL 11

3.1 Introduction 11
3.2 Biodiesel Pilot Performance 12
3.3 Apparent Heat Release Rate 14
3.4 Emissions 20

IV. DUAL-FUEL INVESTIGATIONS: ULTRA-LOW SULFUR DIESEL PILOT FUEL 30

4.1 Introduction 30
4.2 Ultra-Low Sulfur Diesel Pilot Performance 31
4.3 Apparent Heat Release Rate 33
4.4 Emissions 38

IV. CONCLUSIONS 47

5.1 B100 as the Pilot Fuel 47
5.2 ULSD as the Pilot Fuel 49
5.3 ULSD vs. B100 51

REFERENCES 53

APPENDIX

A. AIR-FUEL STOICHIOMETRIC AND MOLE FRACTION CALCULATIONS 56

LIST OF TABLES

2.1. Engine Specifications....6

2.2. Fuel Properties....9

3.1. Experimental Matrix....12

3.2. CA50, SOC, ignition delay, MPRR, and COVimep at PES for Biodiesel....15

4.1. Experimental Matrix....31

4.2. CA50, SOC, ignition delay, MPRR, and COVimep at PES for Ultra-Low Sulfur Diesel....34

LIST OF FIGURES

2.1. Schematic of the 1.9L VW experimental setup 7

3.1. BTE and overall equivalence ratio vs. PES for B100-methane dual fueling 13

3.2. BTE and overall equivalence ratio vs. PES for B100-propane dual fueling 14

3.3. AHRR vs. CAD ATDC at 2.5 bar BMEP.....16

3.4. AHRR vs. CAD ATDC at 5 bar BMEP.....18

3.5. AHRR vs. CAD ATDC at 7.5 bar BMEP.....19

3.6. AHRR vs. CAD ATDC at 10 bar BMEP.....20

3.7. Smoke NO_x tradeoff for straight biodiesel and maximum PES of C_3H_8 and CH_4.....21

3.8. Brake specific NO_x and smoke emissions vs. PES for B100-methane dual fueling 23

3.9. Brake specific NO_x and smoke emissions vs. PES for B100-propane dual fueling 24

3.10. Brake specific CO and CO_2 emissions vs. PES for B100-methane dual fueling 25

3.11. Brake specific CO and CO_2 emissions vs. PES for B100-propane dual fueling 26

3.12. Brake specific THC emissions vs. PES for B100-methane dual fueling.....27

3.13. Brake specific THC emissions vs. PES for B100-propane dual fueling 28

3.14. Brake specific THC emissions vs. $BSNO_x$ tradeoff at various loads and maximum PES for straight biodiesel, B100-methane and B100-propane dual fueling 29

4.1. BTE and overall equivalence ratio vs. PES for ULSD-methane dual fueling 32

4.2. BTE and overall equivalence ratio vs. PES for ULSD-propane dual fueling 33

4.3. AHRR vs. CAD ATDC at 2.5 bar BMEP 35

4.4. AHRR vs. CAD ATDC at 5 bar BMEP 36

4.5. AHRR vs. CAD ATDC at 7.5 bar BMEP 37

4.6. AHRR vs. CAD ATDC at 10 bar BMEP 38

4.7. Smoke NO_x tradeoff for straight biodiesel and maximum PES of C_3H_8 and CH_4 39

4.8. $BSNO_x$ and FSN vs. PES for ULSD-methane dual fueling 40

4.9. $BSNO_x$ and FSN vs. PES for ULSD-propane dual fueling 41

4.10. BSCO and CO_2 emissions vs. PES for ULSD-methane dual fueling 42

4.11. BSCO and CO_2 emissions vs. PES for ULSD-propane dual fueling 43

4.12. Brake specific THC emissions vs. PES for ULSD-methane dual fueling 44

4.13. Brake specific THC emissions vs. PES for ULSD-propane dual fueling 45

4.14. Brake specific THC emissions vs. $BSNO_x$ tradeoff at various loads and maximum PES for straight biodiesel, ULSD-methane and ULSD-propane dual fueling 46

NOMENCLATURE

AHRR	*Apparent Heat Release Rate*
A/F	*Air to Fuel Ratio*
ATDC	*After Top Dead Center*
BMEP	*Brake Mean Effective Pressure*
BSCO	*Brake Specific Carbon-Monoxide*
$BSNO_x$	*Brake Specific Oxides of Nitrogen*
BTE	*Brake Thermal Efficiency*
B100	*Biodiesel*
CAD	*Crank Angle Degree*
CA50	*Crank Angle Corresponding to 50% Heat Release*
C_3H_8	*Propane*
CH_4	*Methane*
CO	*Carbon-Monoxide*
CO_2	*Carbon-Dioxide (percent)*
DAQ	*Data Acquisition*
ECU	*Engine Control Unit*
EGAS	*Exhaust Gas Analysis System*
EGR	*Exhaust Gas Recirculation*

FSN	*Filter Smoke Number*
ID	*Ignition Delay*
LBV	*Laminar Burning Velocity*
LHV	*Lower Heating Value*
$\dot{m}$	*Mass flow rate*
NO_x	*Oxides of Nitrogen*
P	*Pressure*
P_b	*Brake Power*
PES	*Percent Energy Substitution*
PHRR	*Peak Heat Release Rate*
PM	*Particulate Matter*
SOC	*Start of Combustion*
SOI	*Start of Ignition*
TDI	*Turbocharged Direct Injection*
THC	*Total Hydrocarbons (brake-specific)*
VW	*Volkswagen*
V	*Instantaneous Volume*
$\Phi_{overall}$	*Overall Fuel-Air Equivalence Ratio*
γ	*Specific Heat Ratio*

Subscripts:

a	*Air*
bd	*Biodiesel*

g	*Gas (methane or propane)*
l	*Liquid (biodiesel or ultra-low sulfur diesel)*
st	*Stoichiometric*

CHAPTER I

INTRODUCTION

Internal combustion (IC) engines have become an essential part of the modern world and everyday life. They are our primary source of transportation, vital to transnational commerce, and used for backup or onsite power generation. Growing volatility of the oil market along with the growing demands of efficiency and increasingly stringent emission standards has led to interest in different energy sources, such as wind and solar. However, there is no practical replacement for the internal combustion engine since the power density from an internal combustion engine cannot be matched by any of the alternate sources of energy, including, wind, solar, fuel cells, etc. till date. This has provided sufficient motivation for researchers to look for alternate modes of combustion, fuels and fueling strategies to power the internal combustion engine.

Alternate combustion modes, such as homogenous charge compression ignition (HCCI), use a premixed, homogenous mixture of fuel and air that auto-ignites during the compression stroke, have demonstrated promise in improving thermal efficiency and lowering NO_x and soot emissions [1,2] A disadvantage of HCCI is its limited operation range; at low loads HCCI has difficulty auto igniting due to low thermal energy [1] and at high loads HCCI faces high pressure rise rates from volumetric heat release [2].

Dual fueling is a concept that could be implemented with current IC engines in the market. Classical duel fueling uses a gaseous fuel that is inducted along with the intake air, forming a pre-mixed lean fuel-air mixture that is ignited by a liquid pilot fuel injected towards the end of the compression stroke. The primary gaseous fuel typically has a high octane number giving it a high resistance to knock while the liquid pilot fuel usually has a high cetane number giving it a low resistance to auto-ignition. Characteristics of the combustion process in a dual fuel engine depend on the type of primary fuel and its concentration, along with the type of pilot fuel and how it is injected (spray angle, type of injector, etc.). Combustion has been observed in three distinct phases in a dual fuel engine using natural gas as a primary fuel and diesel as the pilot fuel [3]. The first phase involves energy release from the combustion of the diesel pilot; the second consists of the combustion of natural gas in the vicinity of the diesel pilot; and the third phase is due to the combustion of the lean natural gas–air mixture by flame propagation.

Traditionally, dual fuelling was primarily pursued using diesel pilots to ignite natural gas-air mixtures [3-7]. Dual fueling (diesel-natural gas) is not as efficient as straight diesel operation at part loads; however, at higher load conditions, dual fuel performance can equal or surpass straight diesel performance. This is because at high loads the post-ignition combustion phase in conventional diesel operation is mixing controlled; whereas, in classical dual fuel combustion the post-ignition phase is dominated by faster localized turbulent flame propagation in the natural gas-air mixture, which originates from distributed ignition of the diesel pilot. At lower loads, the inefficiency of dual fuel combustion is due to incomplete burn of the premixed natural

gas-air. This also means that there is a high level of total hydrocarbon (THC) and carbon monoxide (CO) emissions at low loads from conventional dual fuel combustion.

Recent experimental demonstrations of advanced low temperature dual fuel concepts [8-13] have re-defined and extended the range of the "classical dual fuel concept [4]" to simultaneously achieve high thermal efficiency and low emissions. The Advanced Low Pilot Ignited Natural Gas (ALPING) combustion concept [8-9] employs very early injection of small diesel pilots (1-5 percent on an energy basis) to ignite lean premixed natural gas-air mixtures to realize very low NO_x emissions and "diesel-like" fuel conversion efficiencies. Kokjohn et al. has demonstrated that very high thermal efficiencies can be achieved with low NO_x and smoke emissions by employing the Reactivity Controlled Compression Ignition (RCCI) concept [10], where a high cetane fuel, diesel, is used to ignite a, low cetane, premixed gasoline-air mixture; and dual-fueling a Premixed Charge Compression Ignition (PCCI) concept, where a premixed mixture of fuel and air auto-ignite during the compression stroke [11-13].

Numerous fuels have been experimentally tested as candidate primary gaseous fuel for dual fuel combustion. These include methane, propane, butane, and hydrogen, among others [14-19]. Several pilot fuels including, diesel, biodiesel and DME have been used to ignite the primary gaseous fuels [20-22]. In this study, the performance, emissions and combustion energy release characteristics of biodiesel-ignited methane (surrogate for natural gas) and biodiesel-ignited propane (surrogate for LPG) along with diesel-ignited methane and diesel-ignited propane combustion are compared in a four cylinder, turbocharged compression fired engine. The diesel used in this study is a pump grade ultra-low sulfur diesel, while the biodiesel used in this study is a soy-derived

methyl ester with a cetane number of 58 (compared to a pump diesel value of 48). Despite its lower (than pump diesel) energy content, the renewable nature of biodiesel and its tendency to reduce particulate matter emissions from combustion make it an excellent replacement candidate fuel to petro-diesel [23-24].

A primary concern of dual fuelling is "end gas knock" at high loads and high substitutions of primary gaseous fuels. Between methane and propane, methane has excellent autoignition-resistant qualities, while propane is more susceptible to knock due to its lower octane rating. Therefore, the maximum energy substitution with propane at high loads is expected to be lower than that obtainable with methane.

The primary objectives of this thesis are,

(1) To compare the performance and emissions characteristics of biodiesel- and diesel-ignited methane and propane combustion over a range of loads and constant engine speed of 1800 rev/min,

(2) To perform detailed investigations of combustion energy release and emissions characteristics of biodiesel and diesel-ignited methane and propane combustion over a range of loads and constant engine speed of 1800 rev/min,

(3) To identify the limits of maximum energy substitution achievable with methane and propane over a range of loads and constant engine speed of 1800 rev/min.

CHAPTER II

EXPERIMENTAL SETUP

All experiments in the present work were performed on a turbocharged direct-injected (TDI), 1.9L, in-line 4-cylinder diesel engine. Relevant engine details are provided in Table 2.1, along with a schematic of the experimental setup in Figure 2.1. The stock ECU of the engine was utilized in the experiments, thus limiting control of the engine. The primary (gaseous) fuel was metered by a manually controlled needle valve, and then introduced along with charge air at the turbocharger intake. Engine speed was controlled with a Froude Hoffman AG80 (Imperial) eddy current dynamometer and engine torque was measured with a calibrated load cell. The ECU controlled biodiesel injection with a throttle position sensor, which was actuated by the Texcel 4.0 dynamometer control software. All gaseous exhaust emissions and smoke were measured downstream of the turbocharger turbine. Gaseous emissions were routed through an emissions sampling trolley to an integrated emissions bench (EGAS2M) manufactured by Altech Environnement S.A and smoke was measured using the AVL 415S variable sampling smoke meter. The stock ECU had shown in previous experiments to provide a negligible amount of exhaust gas recirculation (EGR). Due to the inability to control this parameter of the ECU, the EGR system was deactivated, thereby eliminating an uncontrolled variable.

Table 2.1 Engine Specifications

Engine Type	1997 4-cylinder TDI
Bore x Stroke (mm)	79.5 x 95
Aspiration	Turbocharged
Displacement	1.9 Liters
Nominal compression ratio	19.5:1
Number of valves per cylinder	4
Injection system	Stock mechanical; direct injection
Number of nozzle holes	5
Nominal orifice diameter (μm)	205
Injection timing (static)	4°BTDC

The EGAS2M is a six-gas emissions bench consisting of individual analyzers for simultaneous emissions measurements: (1) a heated flame ionization detector (Graphite 52M) for THC, (2) two chemiluminescent detection cells (Topaze 32M) for NO and NO_x, (3) a non-dispersive infrared analyzer (MIR2M) with different measurement cells for high and low concentrations of CO, exhaust CO_2, O_2, and intake CO_2 (for EGR calculations), and (4) a Fourier Transform Ultra-Violet (FTUV) analyzer for ammonia (NH_3). The AVL 415S smoke meter measured exhaust smoke emissions (expressed as Filter Smoke Number or FSN) using the filter paper method. All data were collected and post-processed (time-averaged) with a modular LabVIEW-based data acquisition system (DAQ) with National Instruments PXI hardware. The measured raw exhaust emissions were converted into brake-specific units by following the standard SAE J1003 procedure with appropriate modifications for biodiesel [25].

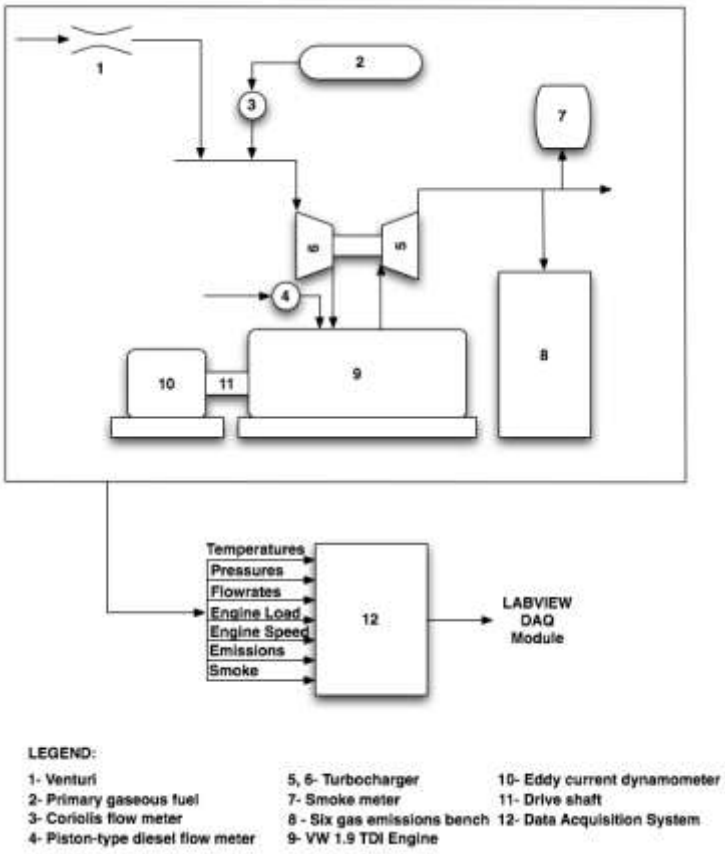

Figure 2.1 Schematic of the 1.9L VW experimental setup

Engine coolant temperatures, pre- and post-turbo air temperatures, intake mixture temperature, and post-turbo exhaust temperatures were measured with Omega Type-K thermocouples. The coolant temperatures were held between 85±2 degrees Celsius, while post turbo intake temperatures were held between 35±2 degrees Celsius. A Micro Motion coriolis mass flow meter with 0.35% accuracy (of reading) was used to measure the mass flow of the primary gaseous fuel. Intake air mass flow rates were measured with a FlowMaxx venturi flow meter. Biodiesel mass flow rate was measured with a Max Machinery Model 213 piston flow meter. Absolute pressure in the test cell was measured with an Omega PX 429 sensor, differential pressure across the venturi flow

meter was measured with a Validyne P55 differential pressure transducer (0.25% accuracy of full scale), and intake boost pressure was measured with a Setra 209 pressure transducer.

In-cylinder pressure was measured in cylinder number one using a Kistler 6056A piezo-electric pressure transducer mounted in a Kistler 6544Q series glow plug adapter. The charge amplifier used was a Kistler 5010B using a medium time constant setting. The glow plug adapter extends into the combustion chamber; therefore, the mounting of the pressure sensor cannot be termed flush in the strictest sense; however, the passage lengths were negligible and did not introduce any extraneous pressure oscillations that could interfere with the fidelity of the cylinder pressure signal; therefore, the pressure sensor was treated as flush mounted for practical purposes. Needle lift was measured using a stock injector that was instrumented with a Wolff needle lift sensor coupled to a signal conditioner. In this work the Start of Injection (SOI) is defined as the crank angle when the injector needle lift reaches 5% of its maximum lift for the cycle. Both in-cylinder pressure and needle lift measurements were recorded with National Instruments PXI S-Series hardware using a BEI encoder of 0.1° crank angle resolution. All in-cylinder data were recorded for 100 successive engine cycles after engine operation attained steady state. To ensure consistency over all cylinder pressure and heat release measurements, the engine was motored for 40 cycles before firing data were taken to ensure that no slippage of the encoder had occurred. Fuel properties of diesel, biodiesel, CH_4, and C_3H_8 are presented in Table 2.2. It should be noted that while the combustion that takes place within the combustion chamber is turbulent the laminar burning velocities of CH_4 and C_3H_8 will affect the turbulent combustion rates.

Table 2.2 Fuel Properties

Parameter	B100	ULSD	Propane	Methane
Purity	N/A	N/A	99.5%	99.97%
Laminar Burning Velocity (LBV)* (cm/s)	N/A	N/A	44.0	40.5
Cetane Number**	58	47.7	N/A	N/A
Octane Number***	N/A	N/A	112	120

*At 1 atm, 298 K and ϕ=1
**Estimated in accordance with ASTM D613 standards
***Published nominal values from Heywood [26]

The engine performance parameters used in this work, such as apparent heat release rate (AHRR) (Joules/degree), along with the specific heat ratio (γ) used in calculating AHRR, pilot equivalence ratio (Φ_{pilot}), overall equivalence ratio (Φ), and percent energy substitution (PES) are defined below.

$$AHRR(q) = \frac{\gamma}{\gamma - 1} P \frac{dV}{dq} + \frac{1}{\gamma - 1} V \frac{dP}{dq} \tag{2.1}$$

$$\gamma(T) = 4.5333 \times 10^{-8} T^2 - 1.74 \times 10^{-4} T + 1.464667 \tag{2.2}$$

$$PES = \frac{\dot{m}_g LHV_g}{\dot{m}_l LHV_l + \dot{m}_g LHV_g} \times 100\% \tag{2.3}$$

$$\phi = \frac{\left(A/F\right)_{st-tot}}{\frac{\dot{m}_a}{\dot{m}_l + \dot{m}_g}} \tag{2.4}$$

$$BTE = \frac{P_B}{\dot{m}_l LHV_l + \dot{m}_g LHV_g} \times 100\% \tag{2.5}$$

In Equations 2.1 through 2.5, P refers to in-cylinder pressure, V refers to the instantaneous volume, T refers to temperature Kelvin, $\dot{m}$ refers to mass flow rates of the liquid pilot fuel (l), gaseous fuel (g), and air (a), and LHV refers to the corresponding lower heating values. Derivatives dV/dq and dP/dq were calculated numerically using a fourth order central difference method. Two different stoichiometric air-fuel ratios were defined: (1) $(A/F)_{st}$ based on the pilot fuel alone, and (2) $(A/F)_{st\text{-}tot}$, which included both the pilot and the main fuels, and was therefore dependent on the primary fuel type (methane or propane) as well as the PES.

Detailed calculations to determine the air-fuel stoichiometric ratio for pilot fuel-primary gaseous fuel combination are provided in the Appendix. A detailed uncertainty analysis was performed in accordance with Kubesh [27] and the maximum uncertainties in brake thermal efficiencies were estimated as 0.803 percent, 0.76 percent and 0.77 percent for B100, B100-propane and B100-methane dual fuelling, respectively.

CHAPTER III

DUAL-FUEL INVESTIGATIONS: BIODIESEL PILOT FUEL

3.1 Introduction

Experiments were conducted on a slightly modified 1.9L, 4 cylinder TDI engine using a dual fueling strategy. Gaseous fuels, propane and methane, were inducted through the pre-turbo air intake and were ignited by a biodiesel (B100) pilot. Performance and emissions data were recorded at four different constant loads at a constant speed of 1800 rev/min. The test matrix for this study is shown in Table 3.1 below. A baseline with biodiesel was established at each load then a gaseous fuel was inducted at different percent energy substitutions (PES). The highest PES was determined by onset of engine instability for each load, except for 10 bar BMEP using propane where the highest PES was determined by the onset of audible knock and/or when the maximum pressure rise rate (MPRR) exceeded 15 bar/CAD with 6 point smoothing. There has been considerable debate about assigning a universal magnitude for MPRR to determine "knock-free" operation. For instance, Yap et al. [28] have used 10 bar/CAD, while Kalghatgi et al [29] have used 7 bar/CAD, and more recently, Hanson et al. [11] have reported MPRR values between 10 bar/CAD to 15 bar/CAD as knock-free, high efficiency conditions for dual fuel operation with pilot diesel and main gasoline fuels. Boost pressure was controlled and kept at the maximum value possible with

baseline B100 operation for every load and PES. The stock ECU limited the amount of EGR to negligible levels; therefore the EGR was valve was closed off and no EGR was used in these experiments.

Table 3.1 Experimental Matrix

Load	BMEP	Methane	Propane
	bar	PES (0-max%)	PES (0-max%)
1/4	2.5	0-71%*	0-64%
2/4	5.0	0-51%	0-50%
3/4	7.5	0-50%	0-49%
4/4	10.0	0-48%	0-43%

*Max PES was decided by the engine instability at lower loads and the onset of audible knock at10 bar BMEP

3.2 Biodiesel Pilot Performance

Four different loads were maintained using a B100-methane dual fuel strategy as observed in Figure 3.1. In general across all PES, the BTE increases with increasing load. The BTE is observed to increase from a baseline value of about 34% to about 35% at maximum PES of 48% at 10 bar BMEP, at 7.5 bar BMEP there seems to be no apparent change in BTE, which stays almost constant at 33%; however, the BTE decreases from the baseline value of about 30% to approximately 28% at 50% PES at 5 bar BMEP and from a baseline value of 25% to approximately 18% at 2.5 bar BMEP, and max PES of 70%. The overall equivalence ratio increases with increasing PES across all the loads.

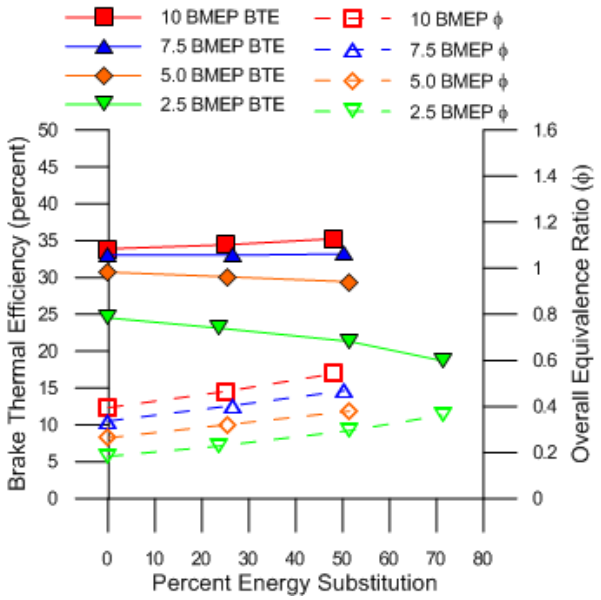

Figure 3.1 BTE and overall equivalence ratio vs. PES for B100-methane dual fueling

As shown on Figure 3.2 similar trends were found when using propane as the inducted gaseous fuel with the following minor changes. The max PES at 10 bar BMEP was 43% as opposed to 48% with methane dual fuelling and the maximum PES at 2.5 bar BMEP reduced from 70% with methane to about 65% with propane dual fuelling. In general, the magnitudes of BTEs were slightly higher with propane than with methane dual fueling. BTE's are better with C_3H_8 with even a slight increase in BTE at 5 bar BMEP and the highest PES. As with CH_4, BTE decreases as higher amounts of C_3H_8 are used at 2.5 bar BMEP and the overall equivalence ratio increases across all the loads as PES increases.

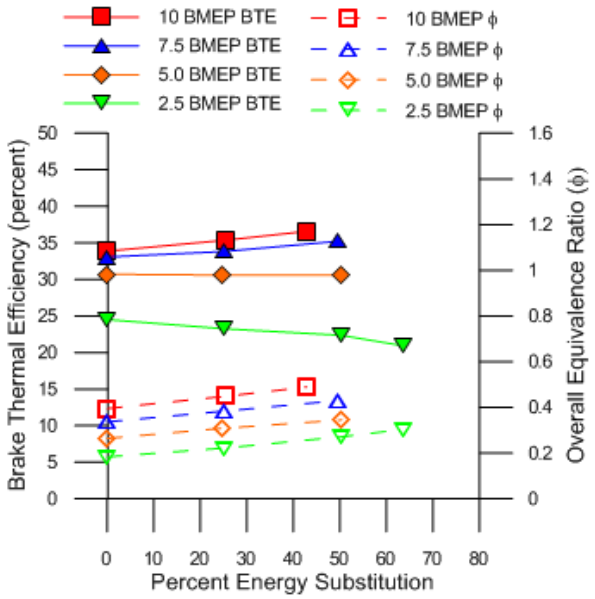

Figure 3.2 BTE and overall equivalence ratio vs. PES for B100-propane dual fueling

3.3 Apparent Heat Release Rate

To better understand the observed performance and emissions trends, apparent heat release rates were calculated as shown in Figures 3.3-3.6. Table 3.2 shows max PES (%), CA50 (CAD ATDC), SOC (CAD BTDC), ignition delay (CAD), SOC (CAD BTDC), maximum pressure rise rate (MPRR) (bar/CAD), boost pressure (psig), and coefficient of variation of indicated mean effective pressure (COVimep) (%) for straight biodiesel, biodiesel-methane, and biodiesel-propane dual fuelling at all four loads.

Table 3.2 CA50, SOC, ignition delay, MPRR, and COVimep at max PES for Biodiesel

BMEP (bar)	2.5			5.0			7.5			10.0		
	B100	CH_4	C_3H_8	B100	CH_4	C_3H_8	B100	CH_4	C_3H_8	B100	CH_4	C_3H_8
Max PES (%)	--	71	64	--	51	50	--	50	49	--	48	43
CA50 (CAD ATDC)	9.5	13.7	12.5	10.6	12.2	10.1	11.8	11.9	7.5	12.7	11.6	6.4
SOC (CAD BTDC)	1.8	1.5	1.6	2.3	2	2.1	2.8	2.4	2.5	3.1	2.7	3.6
Ign. Delay (CAD)	1.2	2.5	1.4	1.7	2.0	1.9	1.2	1.6	1.5	0.9	1.3	0.4
MPRR (bar/CAD)	2.83	2.6	2.8	2.67	2.82	3.18	2.75	2.83	10.04	2.88	3.38	15.23
Boost Pressure (psig)	2.30	2.26	2.23	4.11	3.94	3.79	6.15	5.34	5.57	8.23	7.76	7.14
COVimep (%)	1.24	3.63	2.82	1.1	1.77	0.94	1.00	1.02	0.64	0.94	0.88	0.61

From Table 3.2 it can be seen that for 2.5 bar BMEP the ignition delay and SOC for methane and propane is about the same while biodiesel ignites 0.5 CAD earlier and has a shorter ignition delay. In Figure 3.3, which shows the AHRR schedules for straight B100, B100-propane and B100-methane at max PES of 64% and 71%, respectively, it can be seen that a majority of the fuel burns faster with a higher AHRR for straight biodiesel. While both dual fueling methods have similar AHRR curves the biodiesel-propane fuel mixture has a higher peak AHRR and a faster burn rate than the biodiesel-methane fuel mixture. In general, the combustion energy release seems to occur in two stages, the first comprises of the autoignition of the prepared pilot fuel immediately followed by the subsequent burn of entrained primary gaseous fuel and the second

mixing controlled burn for B100 and by localized flame propagation of the premixed primary gaseous fuel-air mixture for the dual fuel cases. The location of peak heat release rate (PHRR) and CA50 are important parameters that influence the nature of combustion and ultimately the BTE. For instance, the PHRR is progressively retarded from TDC with maximum PES for methane and propane relative to baseline B100 operation. From Table 3.2 it is evident that the phasing of CA50 is most retarded for methane dual fuelling, therefore, it is likely that the corresponding BTE is the lowest. This is because bulk of the combustion energy release occurs during the expansion stroke. This is further confirmed from observations in Figures 3.1 and 3.2 above.

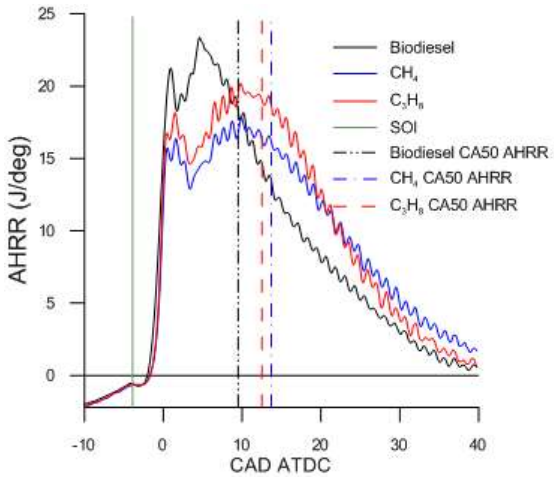

Figure 3.3 AHRR vs. CAD ATDC at 2.5 bar BMEP
Propane and methane are shown at a maximum PES of 64% and 71% respectively

Figure 3.4 shows the AHRR schedules for straight B100, B100-propane and B100-methane at max PES of 50% and 51%, respectively and 5.0 bar BMEP. In general, the magnitude of the first stage energy release due to the autoignition of B100 followed by the immediate consumption of the primary gaseous fuel-air mixture in the vicinity of

the B100 pilot has the same magnitude as that of the 2.5 bar BMEP case; however, the relative magnitude of the mixing controlled energy release for the B100 case, and the energy release from localized flame propagation for B100-propane and B100-methane cases are much higher. The start of combustion is similar for all three fueling methods; however, as shown on Figure 3.4 B100-propane has a higher peak AHRR than straight biodiesel. B100-methane while having the same ignition delay as biodiesel-propane reaches CA50 AHRR 2.1 CAD after B100-propane and 1.6 CAD after straight biodiesel. Clearly, B100-methane exhibits the most retarded CA50, which results in the smallest BTE at the maximum PES. This can be attributed to the slower LBV of methane in comparison to propane. As explained before, bulk of the energy release from combustion in the dual fuel mode occurs via distributed localized flame propagation in the primary gaseous fuel (methane or propane)-air mixture. Although the bulk flame propagation depends on local in-cylinder turbulence, laminar burning velocity (LBV) is a very important factor affecting overall flame propagation at the smallest scales [30]. Therefore, albeit having similar overall equivalence ratios, the CA50 as seen from Table 3.2 for B100-methane combustion is more retarded (by about 2 CAD) than B100-propane combustion at the corresponding maximum PES.

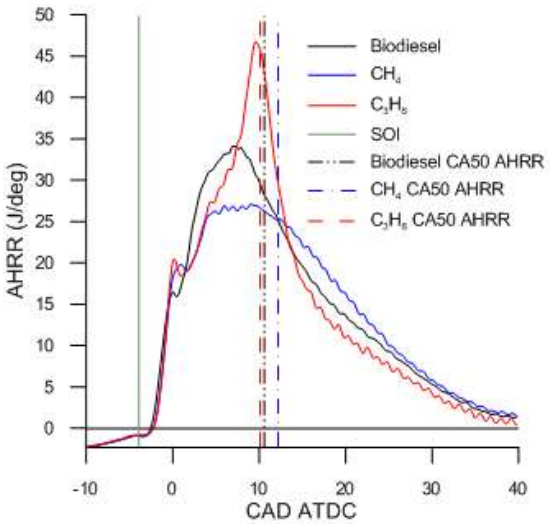

Figure 3.4 AHRR vs. CAD ATDC at 5 bar BMEP

Propane and methane are shown at a maximum PES of 50% and 51% respectively

Figure 3.5 shows the AHRR schedules for straight B100, B100-propane and B100-methane at max PES of 49% and 50%, respectively, and 7.5 bar BMEP. In general, it is seen that bulk of the energy release is dominated by mixing controlled burn for B100, and localized flame propagation for B100-propane and B100-methane dual fuel combustion. Also, the reason for the relatively higher magnitude of PHRR for B100-propane case can be attributed to higher in-cylinder temperatures at higher loads, which may lead to increased turbulent burning velocities; thereby resulting in accelerated energy release rates. In addition, B100-propane records the most advanced CA50 as observed form Table 3.2. While the CA50 phasing for B100-methane and B100 are almost similar, the PHRR for B100 fuelling is of a slightly greater magnitude than for B100-methane combustion. This explains why the BTE for B100 and B100-methane combustion are similar in magnitude at 7.5 bar BMEP, while the BTE for B100-propane at max PES is higher than both baseline B100 and B100-methane in Figures 3.1 and 3.2.

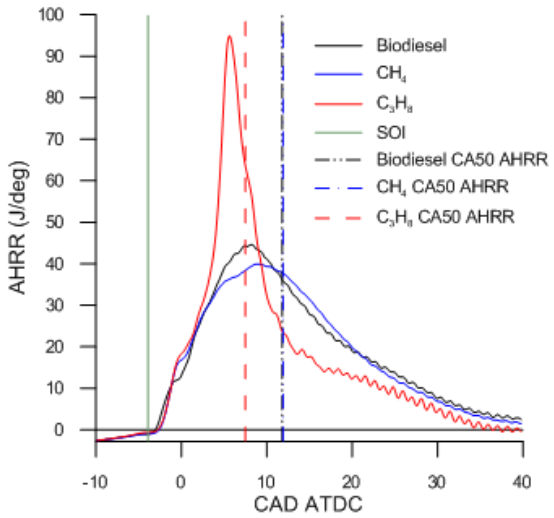

Figure 3.5 AHRR vs. CAD ATDC at 7.5 bar BMEP

Propane and methane are shown at a maximum PES of 49% and 50% respectively

Figure 3.6 shows the AHRR schedules for straight B100, B100-propane and B100-methane at max PES of 43% and 48%, respectively and 10.0 bar BMEP. The order of magnitude of the first stage combustion energy release from autoignition of pilot and entrained primary gaseous fuel is about 20J/deg, which is similar to the 2.5 bar BMEP case. But, the magnitude of the second stage combustion energy release due to localized flame propagation in the primary gaseous fuel-air mixture is much larger; in particular it is highest for B100-propane case. Also, from Table 3.2 it is seen that the CA50 for B100-propane combustion is the most advanced and occurs at 6.4 ATDC; whereas, the CA50 for B100-methane and B100 cases occur at 11.6 and 12.7 CAD ATDC, respectively. These trends of PHRR and CA50 phasing are important parameters that influence the overall nature of combustion, and this is clearly reflected in the BTE trends in Figures 3.1 and 3.2, which shows that B100-propane at maximum PES is the most efficient followed by B100-methane at maximum PES and straight B100 operation. An

important point to note is that the magnitudes of the maximum pressure rise rate, MPRR; from Table 4 is the highest for B100-propane, about 15.23 bar/CAD, which slightly higher than the designated knock limit of 15 bar/CAD. This indicates that operating close to potential knocking conditions would result in the best performance, as indicated by the relatively higher than straight B100 BTE and this also sets the limits of propane substitution at this high load.

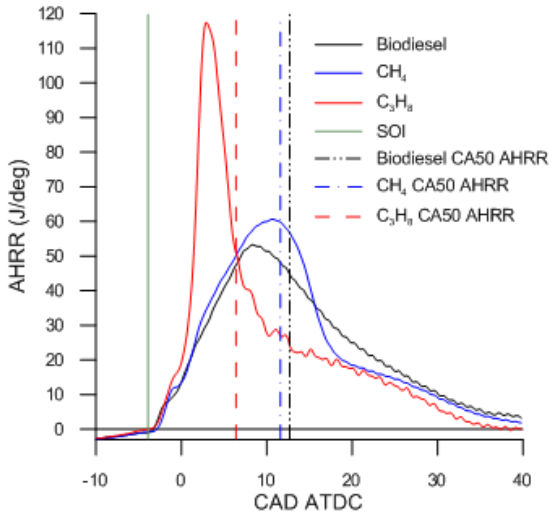

Figure 3.6 AHRR vs. CAD ATDC at 10 bar BMEP

Propane and methane are shown at a maximum PES of 43% and 48% respectively

3.4 Emissions

Figure 3.7 is a smoke-NO_x tradeoff for B100, B100-methane and B100-propane dual fuelling at maximum PES. In general at all loads the smoke and NO_x emissions decrease with increasing PES. It is well known that in straight biodiesel combustion the smoke emissions are tremendously reduced (than corresponding diesel levels), however, the NO_x emissions are expected to be higher than corresponding straight diesel levels (not shown here). The underlying reasons for increased NO_x emissions in B100 combustion is

debatable; however, recent studies by Mueller et al [31] have attributed several reasons including, igniting reacting mixtures that are closer to stoichiometric equivalence ratios leading to higher local temperatures and less radiative losses from the reaction zone due to soot oxidation because of fuel-bound oxygen. In the present study, it is clearly seen that both NO_x and smoke emissions can be simultaneously reduced with increasing methane and propane substitutions. This can be attributed to the fact that at higher gaseous fuel substitutions, the biodiesel spray is progressively reduced in size, i.e. the first stage combustion energy release is from sprays that contain progressively reduced mass of biodiesel; and bulk of the combustion energy release is due to flame propagation in the lean premixed methane- and propane-air mixtures. This leads to lower local temperature, which results in reduced thermal NO_x formation. Additionally, due to the overall lean combustion, smoke emissions are also reduced

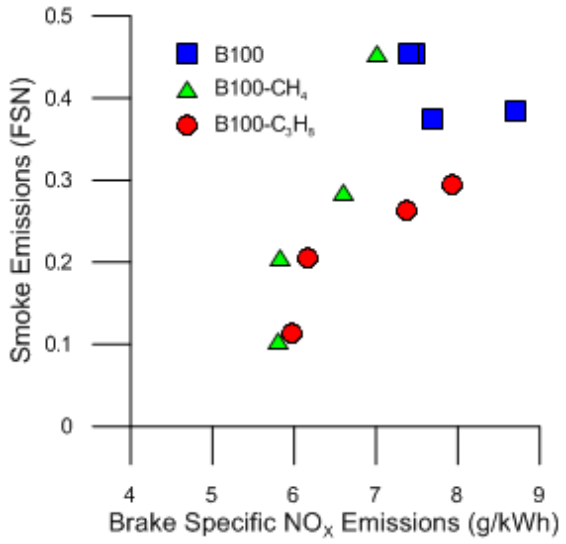

Figure 3.7 Smoke-NO_x tradeoff for straight biodiesel and maximum PES of C_3H_8 and CH_4

Figures 3.8 and 3.9 show the $BSNO_x$ and smoke emissions (FSN) versus PES for B100-methane and B100-propane dual fuel combustion. For B100-methane dual fuelling, in general the $BSNO_x$ decreases with PES for all loads except for the max PES cases at 7.5 bar and 10 bar BMEP. This is because with increasing PES, the biodiesel spray is progressively reduced in size, and this reduces areas inside the cylinder with high local temperatures, which in turn reduces the propensity to form thermal NO emissions. Moreover, the predominantly lean combustion in the surrounding methane-and propane-air mixtures results in further reduction in smoke emissions than with straight B100 combustion. However, for B100-propane combustion, especially at higher loads 7.5 bar and 10 bar BMEP, NO_x emissions are highest at maximum PES. This can be understood from the relative phasing of CA50 at these conditions. As explained above in the AHRR section, the CA50 is most advanced for the 10 bar BMEP case for B100-propane, and the MPRR was about 15.23 bar/deg, which was much higher than the corresponding values at B100, and B100-methane combustion at maximum PES. Due to this, combustion rates are faster, and the residence times for zones with high local temperatures is also high, thereby leading to conditions that favor the formation of thermal NO_x. Whereas, the smoke emissions are consistently lower than B100 levels with increasing propane substitutions; this is because at higher substitutions, bulk of the combustion energy release occurs via localized flame propagation in the lean propane-air mixtures surrounding the B100 spray.

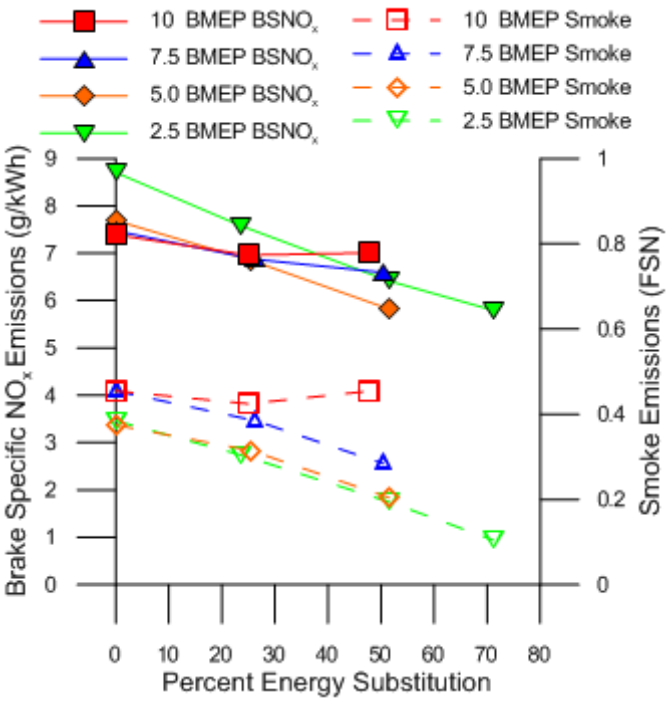

Figure 3.8 Brake specific NO_x and smoke emissions vs. PES for B100-methane dual fueling

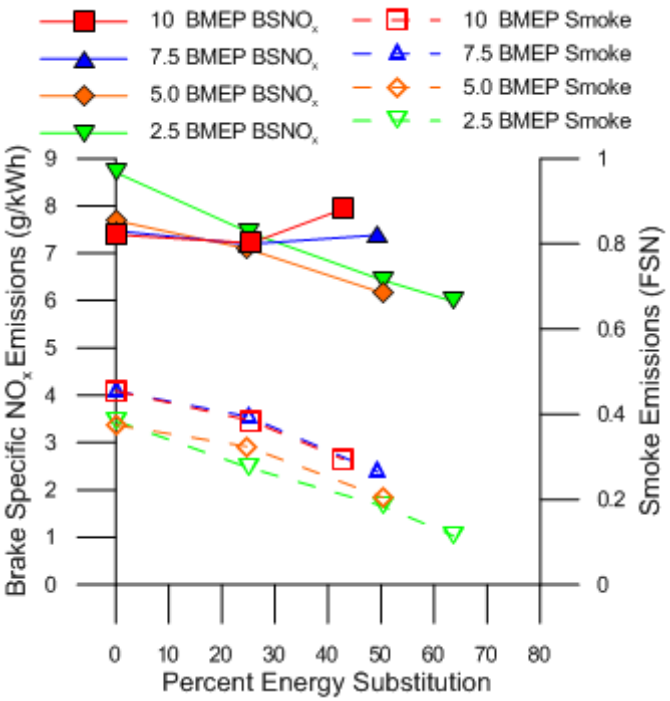

Figure 3.9 $BSNO_x$ and smoke emissions vs. PES for B100-propane dual fueling

Figures 3.10 and 3.11 show BSCO and percent CO_2 emissions versus PES for both B100-methane and B100-propane dual fuel combustion. CO_2 emissions decrease with increasing PES for both B100-methane and B100-propane dual fueling. This is due to the lower carbon content of methane and propane than B100; as the amount of gaseous fuel is increased, the amount of carbon to produce CO_2 decreases.

In general it is seen that CO emissions increase with increasing PES for all loads and decrease with increasing load at all PES. CO originates within the burning pilot and adjoining gaseous regions [3-4]. At lean equivalence ratios, incomplete bulk gas reactions lead to the production of unburned total hydrocarbons (THC) and CO. These incomplete bulk gas reactions occur at low bulk gas temperatures and the CO oxidation (to CO_2) is particularly dependent on bulk gas temperatures [32]. Therefore, it can be

understood that the bulk gas temperatures govern CO emissions, especially at lean equivalence ratios.

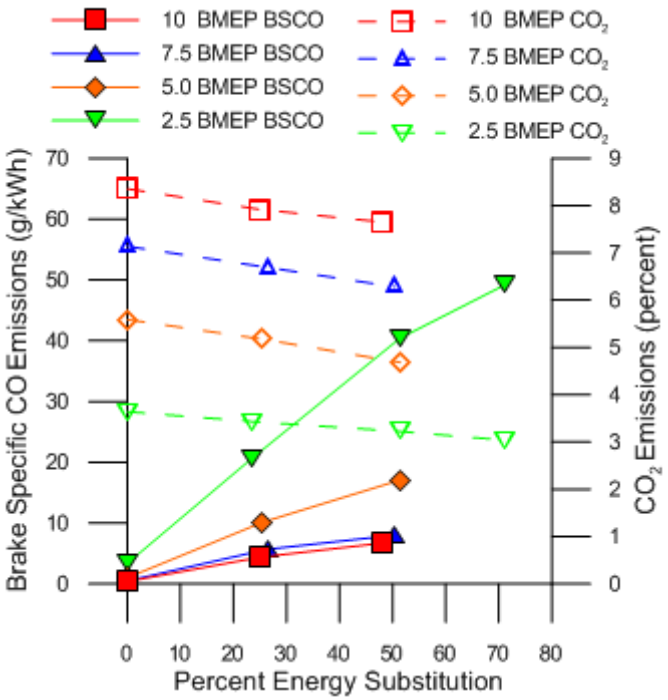

Figure 3.10 Brake specific CO and CO_2 emissions vs. PES for B100-methane dual fueling

With increasing PES at any load in the B100-methane or the B100-propane cases, the bulk gas temperature decreases owing to decreased pilot sizes; therefore, bulk of the combustion energy release occurs via flame propagation in the surrounding leaner than stoichiometric methane or propane-air mixtures.

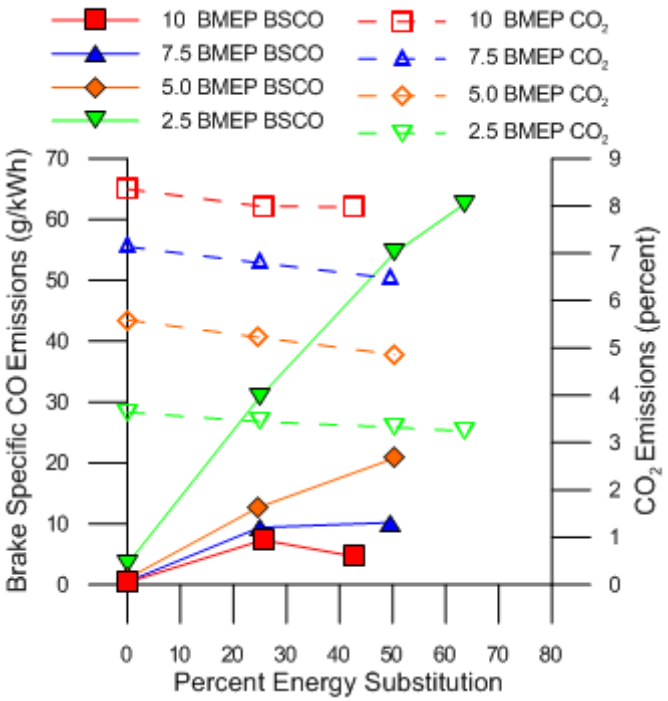

Figure 3.11 Brake specific CO and CO_2 emissions vs. PES for B100-propane dual fueling

There are two important points to note from Figure 3.11, the first being; the BSCO at the 2.5 bar BMEP case for B100-propane combustion is significantly greater than the corresponding B100-methane case, particularly at maximum PES. The second being; at 10 bar BMEP, the BSCO value for the B100-propane case is lower than that of the corresponding B100-methane case. To understand the first observation of increased BSCO with B100-propane in comparison with B100-methane it is instructive to investigate the THC trends at these cases. From Figures 3.12 and 3.13, at 2.5 bar BMEP, particularly at maximum PES, it is seen that the THC for B100-methane is much larger than that for B100-propane combustion. From these THC and CO emissions trends, it can be hypothesized that both fuel (THC) oxidation and CO oxidation are competing reactions. In the case of B100-propane, owing to the fact that propane is easier to oxidize

than methane, fuel oxidation assumes precedence over the relatively slower CO oxidation chemistry. On the other hand, in the case of B100-methane combustion, since methane is more difficult to oxidize, the CO oxidation takes precedence, which is reflected by the overall lower CO emissions accompanied by higher THC emissions.

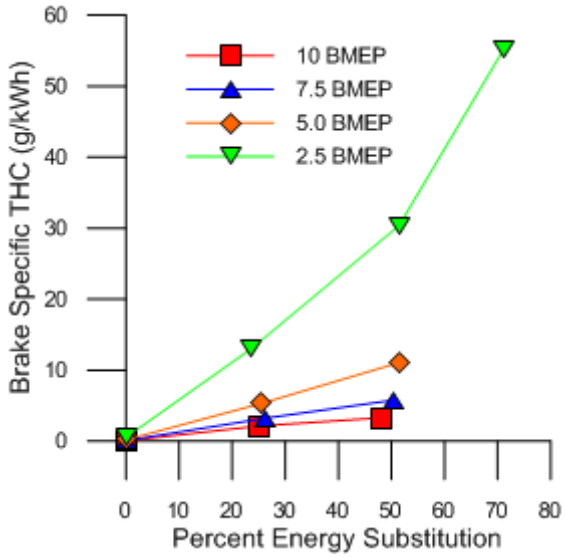

Figure 3.12 Brake specific THC emissions vs. PES for B100-methane dual fueling

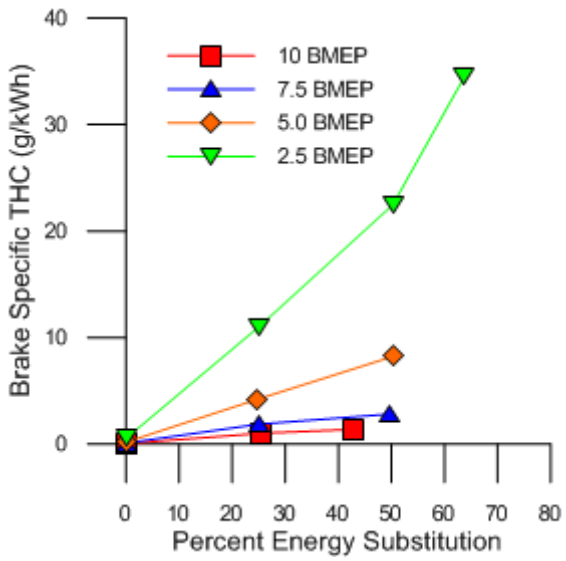

Figure 3.13 Brake specific THC emissions vs. PES for B100-propane dual fueling

Figures 3.12 and 3.13 show the THC emissions trends for B100, B100-methane and B100-propane dual fuel combustion as a function of PES. It can be seen that with increasing PES for both B100-methane and B100-propane combustion, the THC emissions decrease at all loads. In particular, for the 10 bar BMEP case, the THC values for B100-propane combustion are comparable to baseline B100 THC values. Also, the THC magnitudes are lower for B100-propane compared to B100-methane, especially at low loads, 2.5 and 5 bar BMEP. These observations can be explained on the basis of the fact that at 10 bar BMEP, the CA50 is the most advanced for B100-propane combustion, especially at maximum PES. This condition was also characterized by unusually high maximum pressure rise rates (MPRR) of 15.23 bar/CAD. At this condition, the engine was operating very close to knocking conditions and therefore, the combustion is characterized by high local temperatures, which resulted in faster flame propagation speeds, thereby resulting in very low THC emissions. At lower loads, i.e. 2.5 bar and 5

bar BMEP, as explained above, B100-propane had much lower THC emissions compared to B100-methane combustion owing to preferential fuel oxidation in comparison to CO oxidation.

Figure 3.14 is a THC-BSNO$_x$ tradeoff at maximum PES for B100-methane and B100-propane dual fuel combustion at different loads. It can be seen that in general, the BSNO$_x$ increased with increasing load or BMEP with the highest values recorded for straight B100 combustion. The BSNO$_x$ values were observed to decrease with increasing PES with both methane and propane dual fuelling; however, at the lowest loads, the decrease in BSNO$_x$ emissions is accompanied by severe THC penalties. This clearly indicates that at lower loads, the local temperatures are lower, and therefore the NO$_x$ emissions are lower; however, the low temperatures also result in poor THC oxidation.

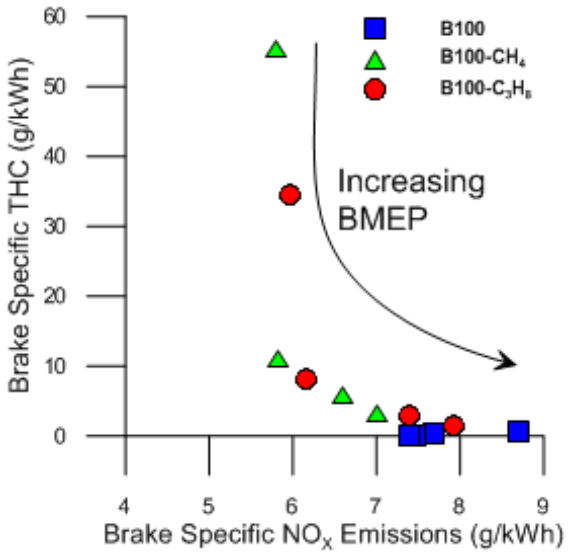

Figure 3.14 Brake specific THC emissions vs. BSNO$_x$ tradeoff at various loads and maximum PES for straight biodiesel, B100-methane and B100-propane dual fueling

CHAPTER IV

DUAL-FUEL INVESTIGATIONS: ULTRA-LOW SULFUR DIESEL PILOT FUEL

4.1 Introduction

To further analyze the effects biodiesel as a pilot fuel in a dual-fueling strategy, the same set of experiments were conducted using ultra-low sulfur diesel (ULSD). Gaseous fuels, propane and methane, were again inducted through the pre-turbo intake with ULSD being used as the pilot fuel. A baseline was established with ULSD, and then the gaseous fuel was inducted for four different loads at a constant speed of 1800 rev/min. The highest PES was again determined by engine instability, except for when propane was being used at10 bar BMEP where the highest PES was determined by audible knock and/or when the MPRR was higher than 15 bar/CAD. Boost pressure was held at its highest point by keeping the waste gate closed and the EGR was closed due to the negligible amount allowed by the stock ECU. The test matrix for this set of experiments is shown in Table 4.1.

Table 4.1 Experimental Matrix

Load	BMEP	Methane	Propane
	bar	PES (0-max%)	PES (0-max%)
1/4	2.5	0-83%*	0-73%
2/4	5.0	0-54%	0-47%
3/4	7.5	0-55%	0-50%
4/4	10.0	0-50%	0-45%

*Max PES was decided by the engine instability at lower loads and the onset of audible knock at10 bar BMEP

4.2 Ultra-Low Sulfur Diesel Pilot Performance

As observed in Figure 4.1 four loads were maintained while increasing PES using an ULSD-methane dual fueling strategy. For all loads BTE decreases with increasing PES. At 10 bar BMEP, the BTE shows a small change dropping from a baseline value of 38% to 37% at the maximum PES of 50%. The 7.5 bar BMEP and 5 bar BMEP loads show similar, albeit slightly larger drops with a drop from 37% baseline to approximately 35% at a maximum PES of 35% for 7.5 bar BMEP and 35% baseline to approximately 31% at a maximum PES of 54% for 5 bar BMEP. The largest BTE drop is at 2.5 bar BMEP, with 27% baseline to approximately 16% at a maximum PES of 83%. Overall equivalence ratios increase for increasing loads and with increasing PES.

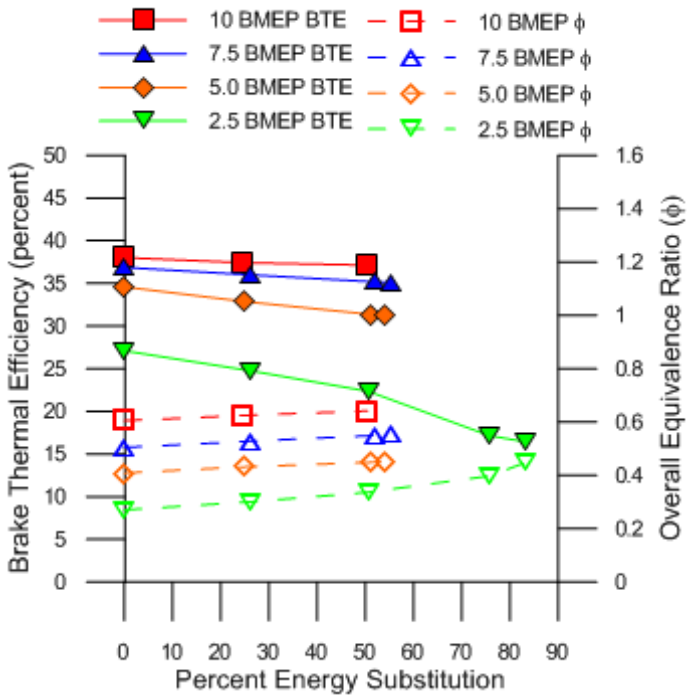

Figure 4.1 BTE and overall equivalence ratio vs. PES for ULSD-methane dual fueling

Observing Figure 4.2, ULSD-propane shows a slight increase in BTE with increasing PES at 10 bar BMEP, while showing a decrease in BTE with increasing PES at lower loads similar to that of ULSD-methane dual fueling as seen in Figure 4.1. It should also be noted with propane the maximum amount of PES decreased for every load but 7.5 bar BMEP where both maximum PES for propane and methane were the same. At 7.5 bar BMEP, BTE stayed a 37% from baseline to a maximum PES of 50%. The BTE showed an increase at 10 bar BMEP from 38% baseline to approximately 39% at a maximum PES of 45 %. Again overall equivalence ratio increased with higher loads and increasing PES.

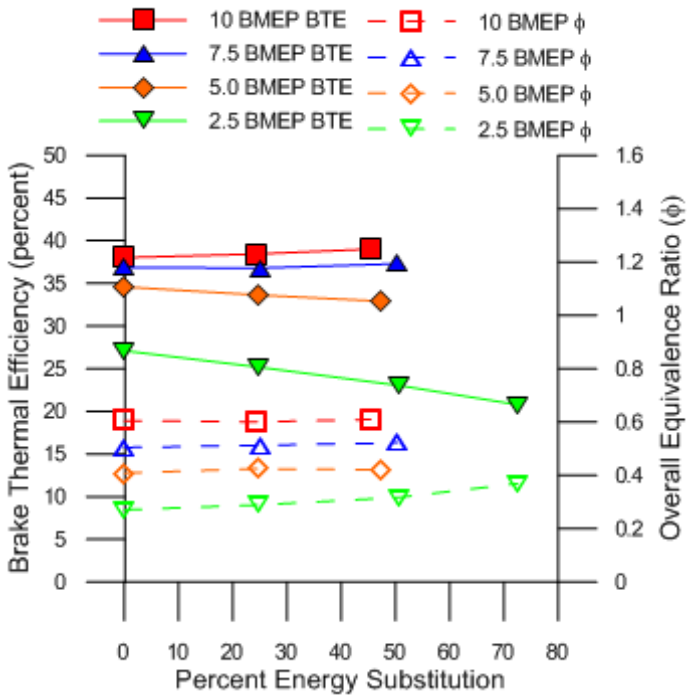

Figure 4.2 BTE and overall equivalence ratio vs. PES for ULSD-propane dual fueling

4.3 Apparent Heat Release Rate

To further understand performance and emission trends, apparent heat release rate (AHRR) trends were calculated and presented in Figures 4.3-.4.6. Table 4.2 presents max PES (%), CA50 (CAD ATDC), SOC (CAD BTDC), ignition delay (CAD), SOC (CAD BTDC), maximum pressure rise rate (MPRR) (bar/CAD), boost pressure (psig), and coefficient of variation of indicated mean effective pressure (COVimep) (%) for straight ULSD, ULSD-methane, and ULSD-propane dual fuelling at all four loads. It can be seen from Table 4.2 at 2.5 bar BMEP the ignition delay for methane and propane is comparatively the same and about 0.5 CAD larger than ULSD's ignition delay.

Table 4.2 CA50, SOC, ignition delay, MPRR, and COVimep at max PES for Ultra-Low Sulfur Diesel

BMEP (bar)	2.5			5.0			7.5			10.0		
	ULSD	CH_4	C_3H_8	ULSD	CH_4	C_3H_8	ULSD	CH_4	C_3H_8	ULSD	CH_4	C_3H_8
Max PES (%)	--	83	73	--	54	47	--	55	50	--	50	45
CA50 (CAD ATDC)	10.2	15.4	13.5	11.2	13.3	10.1	12.8	13	7.8	13.6	12.4	6.9
SOC (CAD BTDC)	0.5	0.8	0.3	0.6	0.1	0.1	1.3	0.4	1.6	1.9	1.2	2.4
Ign. Delay (CAD)	2.8	3.4	3.3	2.9	3.4	3.4	2.4	2.9	1.9	2	2.5	1.7
MPRR (bar/CAD)	4.37	2.03	3.07	5.37	5.65	6.17	4.69	6.01	10	4.17	5.42	13.73
Boost Pressure (psig)	2.58	2.91	2.64	4.32	4.04	3.87	6.28	5.70	5.46	8.69	7.78	7.36
COVimep (%)	1.34	4.65	2.95	0.92	1.37	1.09	1.05	0.9	0.61	0.99	0.88	3.77

The AHRRs in Figure 4.3 show a higher peak heat release rate (PHRR) for diesel and an earlier CA50 then with propane and methane which have a later PHRR and CA50. The AHRR for propane and methane show a somewhat similar curve with AHRR peaking from autoignition of the diesel pilot and then a smaller peak from the premixed primary gaseous fuel-air mixture. Observing CA50 for methane it is seen that it is about 2 CADs more retarded then CA50 for propane and 5 CADs more retarded then straight ULSD. As explained in the previous chapter this is because a majority of the combustion energy is released during the expansion stroke, leading to the lower BTEs seen in Figures 4.1 and 4.2.

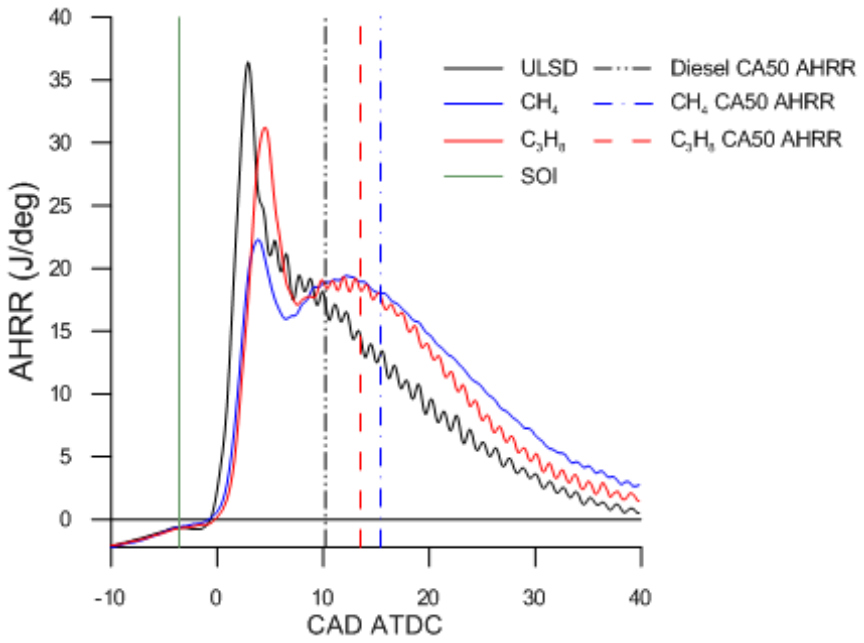

Figure 4.3 AHRR vs. CAD ATDC at 2.5 bar BMEP

Propane and methane are shown at a maximum PES of 77% and 83% respectively

Figure 4.4 presents AHRR curves for straight ULSD, propane and methane at 5.0 bar BMEP. It is evident that all three fueling strategies have a 1st stage AHRR peak and then a 2nd stage AHRR peak, although methane has a much smaller 2nd stage AHRR peak. Ignition delay is the same for propane and methane for 5.0 bar BMEP as shown in Table 4.2 and as with 2.5 bar BMEP straight ULSD shows a shorter ignition delay than both propane and methane. However, even with the longer ignition delay, propane CA50 is advanced 1.0 CAD before straight ULSD and propane has a much higher 2nd stage AHRR peak than the other fueling strategies; this is likely due to the higher laminar burning velocity of propane.

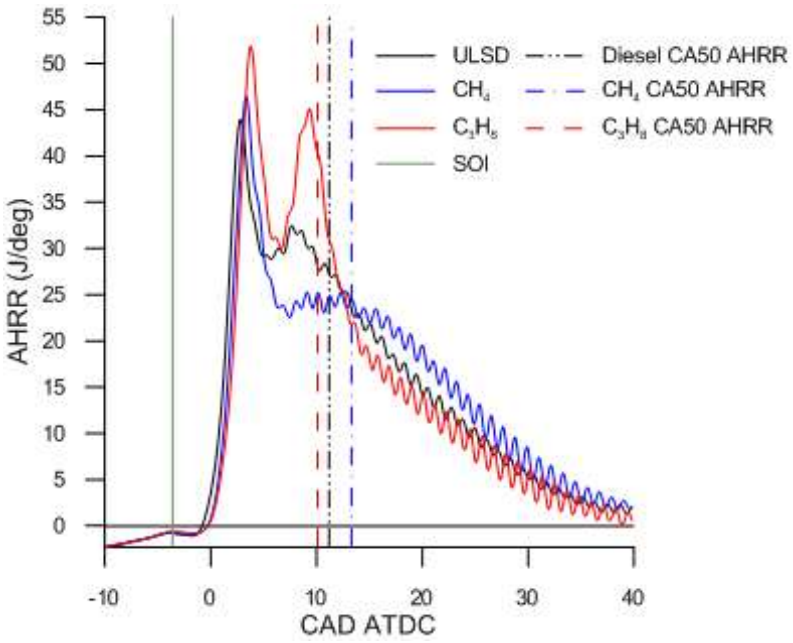

Figure 4.4 AHRR vs. CAD ATDC at 5 bar BMEP

Propane and methane are shown at a maximum PES of 47% and 54% respectively

Figure 4.5 shows the AHRR schedules at 7.5 bar BMEP for straight ULSD, ULSD-propane, and ULSD-methane at max PES 50% and 54% respectively. At 7.5 bar BMEP Table 4.2 shows that ignition delay for ULSD-methane and straight ULSD both decrease by 0.5 CAD while ignition delay for ULSD-propane decreases by 1.5 CAD making it smaller than the ignition delay for straight ULSD. Again all three fuels demonstrate two peaks typically found in CI engines, although propane demonstrates a much higher 2nd stage AHRR peak then typical straight ULSD and methane shows a lower 2nd stage AHRR peak then straight ULSD. The PHRR for ULSD-propane is substantially higher than ULSD-methane and straight ULSD, leading to CA50 being reached about 5 CAD faster than both other fueling methods.

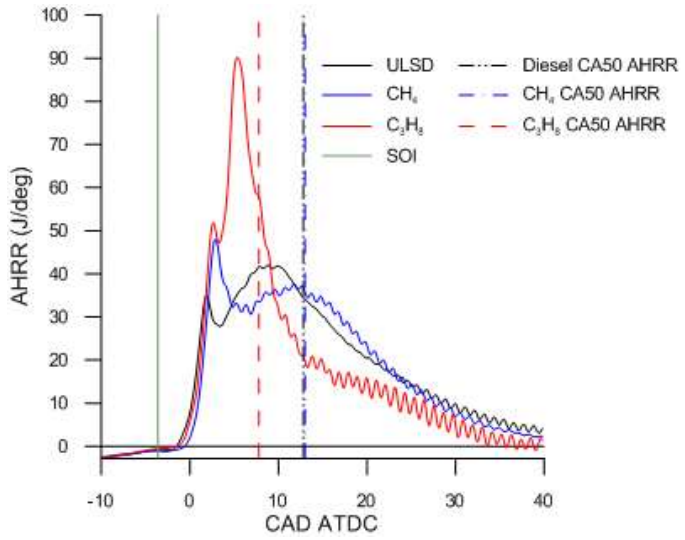

Figure 4.5 AHRR vs. CAD ATDC at 7.5 bar BMEP

Propane and methane are shown at a maximum PES of 50% and 54% respectively

Figure 4.6 shows the AHRR schedules at 10 bar BMEP for straight ULSD, ULSD-propane, and ULSD-methane at maximum PES 45% and 50% respectively. At this point only the straight ULSD and ULSD-methane AHRR curves look similar, albeit ULSD-methane with a higher PHRR; both fueling methods demonstrate a smaller 1st stage AHRR peak followed by a larger 2nd stage AHRR peak, which is typical for a CI engine at higher loads. It should also be noted that from Table 4.2 ULSD-methane reaches CA50 at 12.4 CAD which is advanced just over 1.0 CAD of straight ULSD at 13.6 CAD. In the case of ULSD-propane there is no 2nd stage AHRR peak, due to increased pilot sizes and ignition sites, which results in overall increased burn rates. This leads to a very advanced CA50 at 6.9 CAD and a very high PHRR. The advanced CA50 of ULSD-propane leads to a slightly higher BTE over straight ULSD as seen in Figure 4.2; however, when observing Figure 4.1 it can be seen that the BTE for ULSD-methane never gets above that of straight ULSD, even though the CA50 is slightly more advanced.

Another item to note is because of the high PHRR of ULSD-propane the MPRR is13.73 bar/CAD as seen in Table 4.2. This high MPRR is close to the designated knock limit of 15 bar/CAD.

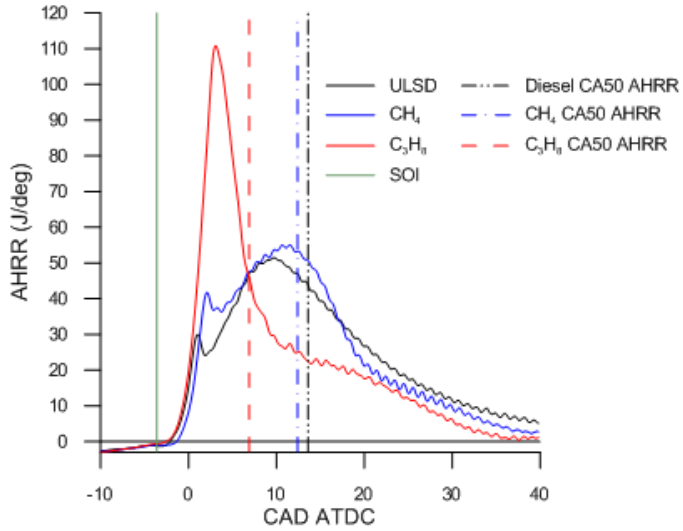

Figure 4.6 AHRR vs. CAD ATDC at 10 bar BMEP

Propane and methane are shown at a maximum PES of 45% and 50% respectively

4.4 Emissions

Smoke-NO_x tradeoffs for ULSD, ULSD-propane, and ULSD-methane are presented in Figure 4.7. Smoke and NO_x emissions generally decrease with increasing PES independent of the load. The lower smoke numbers can be attributed to the higher gaseous fuel substitutions.

This can be attributed to the fact that at higher gaseous fuel substitutions, the diesel spray is progressively reduced in size, i.e. the first stage combustion energy release is from sprays that contain progressively reduced mass of diesel; and bulk of the combustion energy release is due to flame propagation in the lean premixed methane- and

propane-air mixtures. This leads to lower local temperature, which results in reduced thermal NO_x formation. Additionally, due to the overall lean combustion, smoke emissions are also reduced.

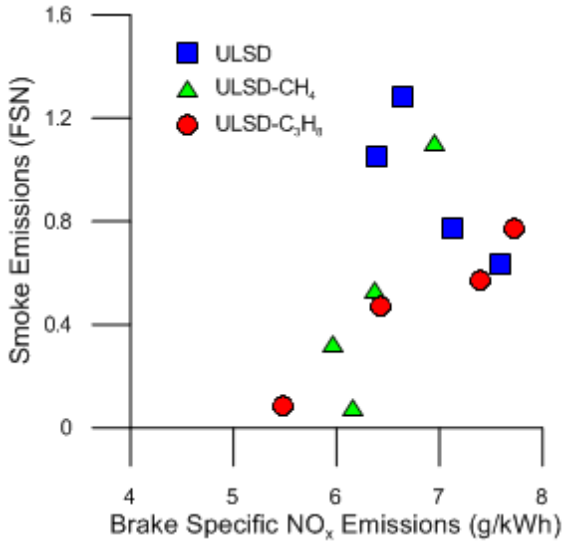

Figure 4.7 Smoke-NO_x tradeoff for straight ULSD and maximum PES of C_3H_8 and CH_4

$BSNO_x$ and FSN vs. PES are shown in Figures 4.8 and 4.9 for straight ULSD, ULSD-methane, and ULSD-propane. At most loads $BSNO_x$ decreases as PES is increased for ULSD-methane dual fueling; the exceptions being 50% PES and above at 7.5 bar BMEP and 10 bar BMEP; and 75% PES at 2.5 bar BMEP. The same trend is observed for ULSD-propane dual fueling, sans any outlier points. The decrease in $BSNO_x$ emissions as PES increases is due most likely due to the decreased diesel sprays as PES is increased. The uncharacteristic high point at 75% PES for 2.5 bar BMEP, is possibly from the difficulty of keeping the VW at the correct load at that point. Due to the difficulty of controlling the pilot fuel a slightly smaller load point of 2.3 bar BMEP was used at 75% PES. The higher $BSNO_x$ emissions for 7.5 bar BMEP and 10 bar BMEP at

the higher PES are possibly due to the MPRR and local temperatures at these points. Although CA50 is close to the same at these points for straight ULSD and USLD-methane the MPRR is noticeably larger for ULSD-methane and along with observing Figures 4.5 and 4.6 it may be said that the initial combustion rates of ULSD-methane are faster, possibly supporting local residence zones with high temperatures leading to favorable thermal NO_x formation. The same can be more easily said with ULSD-propane dual fueling with its MPRR bordering on knock at and advanced CA50 leading to a high amount of local residence zones with high temperatures.

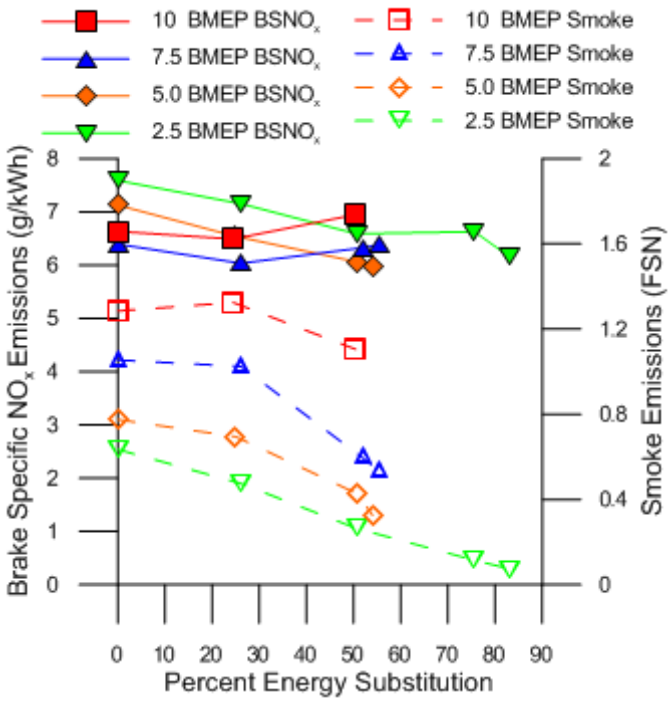

Figure 4.8 $BSNO_x$ and smoke emissions vs. PES for ULSD-methane dual fueling.

FSN emissions decrease for both ULSD-methane and ULSD-propane with increasing PES. This is due to the ascendancy of the lean fuel air mixture combustion as the PES of both methane and propane are increased.

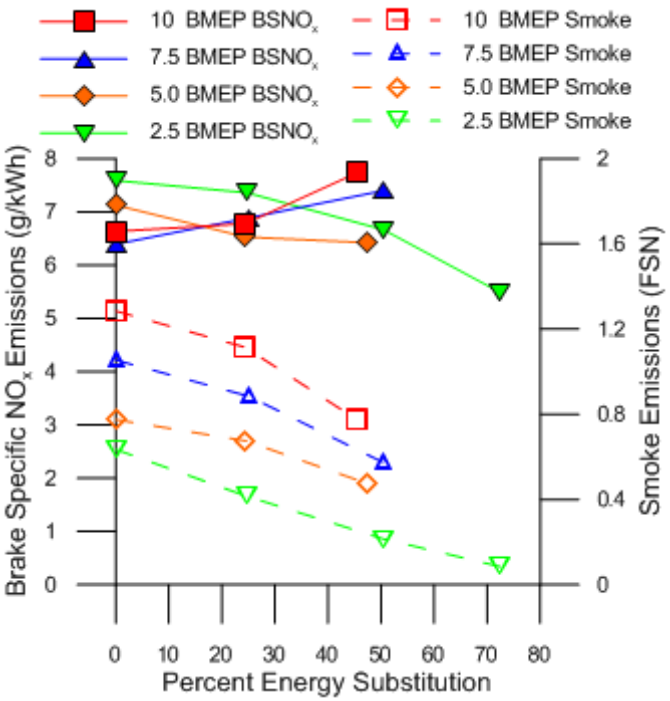

Figure 4.9 $BSNO_x$ and smoke emissions vs. PES for ULSD-propane dual fueling

Figure 4.10 and 4.11 show BSCO and percent CO_2 emissions versus PES for both ULSD-methane and ULSD-propane dual fuel combustion. CO_2 emissions decrease as PES is increased at all loads and for both types of dual fueling. This is due to the lower carbon content of methane and propane than ULSD; as the amount of gaseous fuel is increased, the amount of carbon to produce CO_2 decreases.

It can be seen that most CO emissions increase with increasing PES, save the maximum PES at 2.5 bar BMEP for ULSD-methane and the maximum PES at 10 bar BMEP for ULSD-propane. Overall CO emissions for ULSD-propane are higher than ULSD-methane, except for the maximum PES's at 10 bar BMEP.

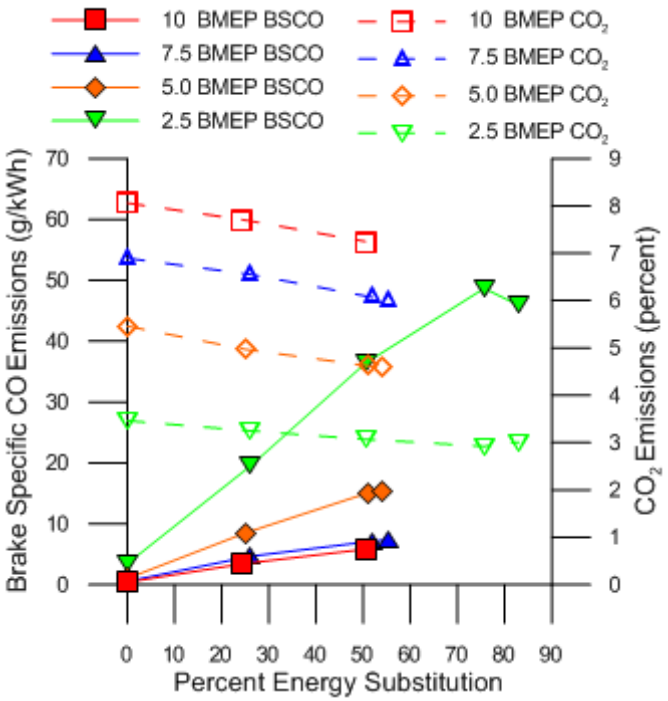

Figure 4.10 BSCO and CO_2 emissions vs. PES for ULSD-methane dual fueling

The increase in CO is due because as PES is increased, pilot fuel decreases and more of the combustion energy is carried by the lean mixture of air and primary fuel. With a rise of the combustion energy being carried by flame propagation within the air-fuel mixture there is a decrease in bulk gas temperatures. Since CO oxidation is governed by chemical kinetics, which is a product of the bulk gas temperatures and therefore increases as the bulk temperature is decreased [3-4].

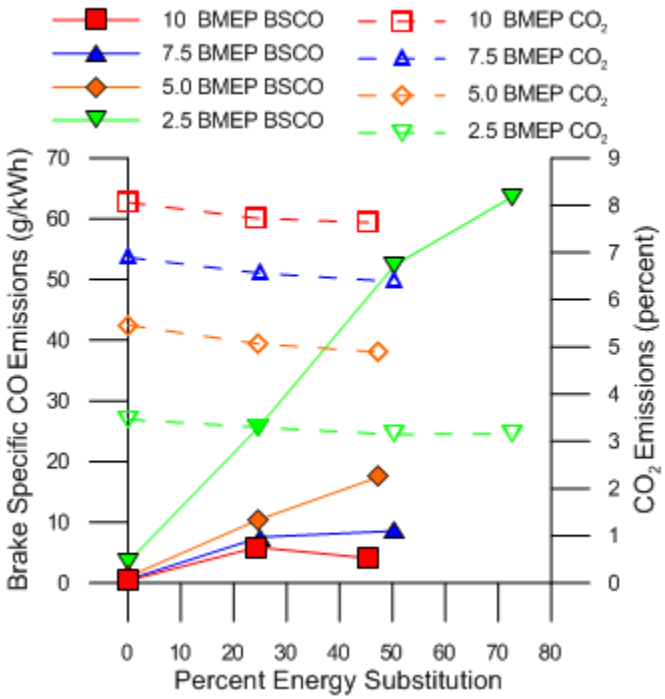

Figure 4.11 BSCO and CO_2 emissions vs. PES for ULSD-propane dual fueling

At 2.5 bar BMEP, the BSCO emissions are observed to increase due to increased gaseous substitutions. As a result bulk gas temperatures are lower and this when combined with overall lean equivalence ratios, results in high CO emissions. THC emissions need to be observed to understand why ULSD-propane has higher BSCO emissions then ULSD-methane at all the other points.

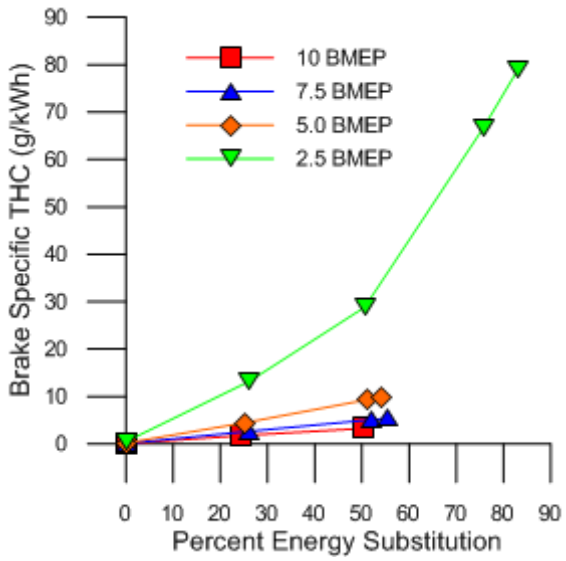

Figure 4.12 Brake specific THC emissions vs. PES for ULSD-methane dual fueling

Figures 4.12 and 4.13 present brake specific THC vs. PES for ULSD-CH_4 and ULSD-C_3H_8 dual fueling. Overall as PES is increased so does THC emissions and THC emissions for ULSD-methane are much higher than ULSD-propane. This is likely due to propane being easier to oxidize than methane. As discussed in Chapter 3 when observing BSCO and THC emissions it can be theorized that CO oxidation and THC oxidation are competing reactions. With methane being more difficult to oxidize, CO oxidation takes precedence thereby producing less CO emissions than propane.

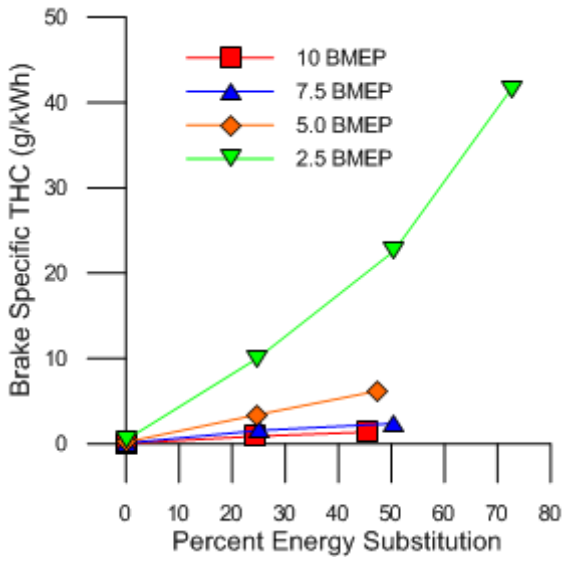

Figure 4.13 Brake specific THC emissions vs. PES for ULSD-propane dual fueling

Figures 4.13 and 4.14 show the THC emissions for straight ULSD, ULSD-methane and ULSD-propane. It can be seen that THC emissions increase with increasing PES for both ULSD-methane and ULSD-propane. THC emissions for ULSD-methane are higher than THC emissions for ULSD-propane across all loads and for all PES. This is best characterized at lower loads, in particular at maximum PES at 2.5 bar BMEP. At these lower loads it can be assumed that the previous explanation of THC being a competing reaction to CO explains the lower THC emissions for ULSD-propane. At higher loads the lower THC emissions for ULSD-propane can be explained by observing maximum PES at 10 bar BMEP, where CA50 is 6.9 CAD and MPRR is close to knock at 13.73 bar/CAD. Because the engine is running close to knock, combustion is characterized by high local temperatures, resulting in faster flame propagation which leads to lower THC emissions.

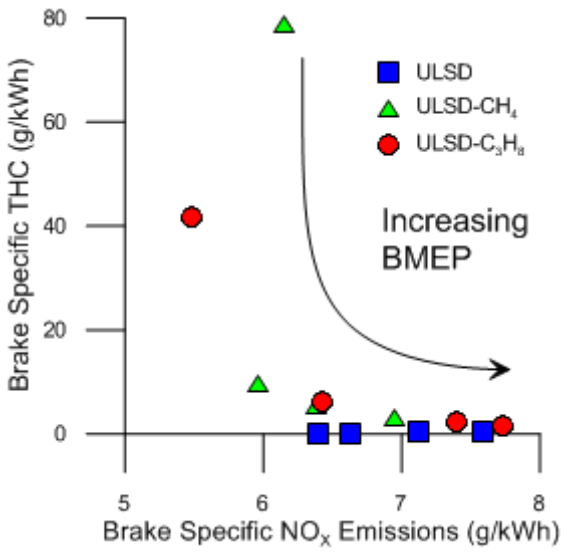

Figure 4.14 Brake specific THC emissions vs. $BSNO_x$ tradeoff at various loads and maximum PES for straight ULSD, ULSD-methane and ULSD-propane dual fueling

Figure 4.14 shows the tradeoff between THC vs. $BSNO_x$ for straight ULSD, ULSD-methane, and ULSD-propane at maximum PES. In general NO_x emissions increase with increasing load when the primary fuel is at its maximum PES, it can be seen the highest $BSNO_x$ emissions are for the maximum PES of propane at 10 bar BMEP. NO_x emissions are likely low at lower loads while THC emissions are high due to low local temperatures at lower loads leading to low NO_x, but also to poor THC oxidation.

CHAPTER V

CONCLUSIONS

Performance and emissions data were obtained from dual fueling experiments on an inline, 4 cylinder turbocharged compression ignition engine (with stock ECU and wastegated turbocharger) fueled with straight biodiesel (B100), straight ultra-low sulfur diesel (ULSD), and B100-propane, B100-methane, ULSD-propane, and ULSD-methane dual fuel combustion over a range of loads (2.5-10 bar BMEP) and percent energy substitution (PES) at 1800 rev/min. The following conclusions can be made from the experimental results presented in this work.

5.1 B100 as the Pilot Fuel

1. Maximum PES levels were restricted to 70% at 2.5 bar BMEP and 48% at 10 bar BMEP for B100-methane dual fuelling and 65% at 2.5 bar BMEP and 43% at 10 bar BMEP for B100-propane dual fuelling. The maximum PES was limited by misfire at 2.5 bar BMEP and by the onset of audible engine knock or when the maximum pressure rise rate (MPRR) exceeded 15 bar/CAD at 10 bar BMEP.
2. At maximum PES, the BTEs for both B100-methane and B100-propane dual fuelling at 2.5 bar BMEP was about 5-6 percentage points lower than

baseline B100 values but approached or slightly exceeded (by about 1.0-1.5 percentage points) at 10 bar BMEP.

3. The CA50 phasing was identified as an important parameter to understand the nature of dual fuel combustion relative to straight B100 combustion. For instance, at 10 bar BMEP and maximum PES, the CA50 phasing was the most advanced for B100-propane case, 6.4 CAD ATDC, which is about 6.3 CAD more advanced than for straight B100 fuelling. This observation was consistent with the fact that the B100-propane BTE at maximum PES and 10 bar BMEP was the highest at about 36%. This advanced CA50 phasing also led to increased NO_x emissions since the local combustion temperatures were likely higher for a longer time, promoting the formation of thermal NO_x.
4. The $BSNO_x$ vs. PES, smoke vs. PES trends, and the smoke-NO_x tradeoffs at maximum PES indicate that in general, the B100-methane and B100-propane dual fuelling strategies were beneficial in reducing both NO_x and smoke emissions at all reported loads with maximum benefits at low loads. For example, the NO_x emissions decreased by about 33% and the smoke emissions decreased by about 50% from corresponding baseline (B100) values at maximum PES for both B100-methane and B100-propane dual fuel combustion at 2.5 bar BMEP.
5. The THC vs. PES, BSCO vs. PES indicate that both THC and CO emissions decrease with increasing loads at all PES, and that at any load, both THC and CO emissions increased with PES for both B100-methane

and B100-propane dual fuel combustion. For example at 2.5 bar BMEP BSCO and THC emissions increase of 93.1% and 99% respectively with methane as the primary fuel and an increase of 94.6% and 98.5% respectively with propane as the primary fuel. However, BSCO and THC emissions decrease from 2.5 bar BMEP to 10 bar BMEP by 86.4% and 94.1% respectively with maximum PES of methane and a decrease of 91.5% and 96% respectively with maximum PES of propane.

5.2 ULSD as the Pilot Fuel

1. Maximum PES levels were restricted to 83% at 2.5 bar BMEP and 45% at 10 bar BMEP for ULSD-methane dual fuelling and 73% at 2.5 bar BMEP and 45% at 10 bar BMEP for ULSD-propane dual fuelling. The maximum PES was limited by misfire at 2.5 bar BMEP and by the onset of audible engine knock or when the maximum pressure rise rate or MPRR exceeded 15 bar/CAD at 10 bar BMEP.
2. At maximum PES, the BTEs for both ULSD-methane and ULSD-propane dual fuelling at 2.5 bar BMEP were about 7-10 percentage points lower than baseline ULSD values but approached within 1 percentage point for ULSD-methane and slightly exceeded by about 1.0-1.5 percentage points for ULSD-propane at 10 bar BMEP.
3. Similar to the B100 experiments, the CA50 phasing was an important parameter for ULSD as a pilot fuel too. For instance, at 10 bar BMEP and maximum PES, the CA50 phasing was the most advanced for ULSD-

propane case, 6.9 CAD ATDC, which is about 6.7 CAD more advanced than for straight ULSD fuelling. This observation was consistent with the fact that the ULSD-propane BTE at maximum PES and 10 bar BMEP was the highest at about 36%. This advanced CA50 phasing also led to increased NO_x emissions since the local combustion temperatures would be higher for a longer time, promoting the formation of thermal NO_x.

4. The $BSNO_x$ vs. PES, smoke vs. PES trends, and the smoke-NO_x tradeoffs at maximum PES indicate that in general, the ULSD-methane and ULSD-propane dual fuelling strategies were beneficial in reducing both NO_x and smoke emissions at all reported loads with maximum benefits at low loads. For example, the NO_x emissions decreased by about 19% to 28% for ULSD-methane and ULSD-propane respectively; while smoke emissions decreased by about 87% from corresponding baseline (USLD) values at maximum PES for both ULSD-methane and USLD-propane dual fuel combustion at 2.5 bar BMEP.
5. The THC vs. PES, BSCO vs. PES indicate that both THC and CO emissions decrease with increasing loads at all PES, and that at any load, both THC and CO emissions increased with PES for both ULSD-methane and ULSD-propane dual fuel combustion. For example at 2.5 bar BMEP BSCO and THC emissions increase of 92.5% and 99.4% respectively with methane as the primary fuel and an increase of 94.6% and 98.8% respectively with propane as the primary fuel. However, BSCO and THC emissions decrease from 2.5 bar BMEP to 10 bar BMEP by 87.3% and

95.9% respectively with maximum PES of methane and a decrease of 93.6% and 96.7% respectively with maximum PES of propane.

5.3 ULSD vs. B100

1. The SOI remained within 0.5 CAD in most cases for both B100 and ULSD; but due to B100's higher cetane number, ignition delay was shorter and CA50 was more advanced for B100. However, examining the AHRR it can be seen that even though ULSD has a more retarded CA50 than B100, a bulk of its combustion energy is released in the 1st stage AHRR peak near top dead center; making ULSD more efficient as a baseline and pilot fuel.
2. Tables 3.2 and 4.2 indicate than ULSD was able to achieve a higher PES than B100 at virtually every load for both methane and propane; this is likely due to the higher cetane number of B100, making B100 more ignitable. This is further indicated when considering the ignition delays also seen in Tables 3.2 and 4.2; where B100 has a shorter ignition delay than ULSD for every load and PES for methane and propane.
3. As discussed in the introduction B100 produces less smoke than ULSD; this also holds true when B100 is used as the pilot fuel However, B100 as a pilot fuel led to overall higher CO,CO_2, NO_x, and THC emissions.
4. When ULSD is used as a pilot fuel the MPRR is for the most part higher than when B100 is used as the pilot fuel. Comparing Figures 3.3-3.6 to Figures 4.3-4.6 it can be seen that ULSD has a much higher 1st stage

AHRR peak than B100, which leads to the overall higher MPRR and quicker CA50 seen when using ULSD as a pilot fuel.

5. The THC vs. BSNOx tradeoff at maximum PES indicated that in general dual fuelling was beneficial in reducing NOx emissions from baseline B100 and ULSD values at all loads; however, the THC penalties were high, especially at low loads.
6. Due to the lower carbon content of methane and propane dual-fueling was found to be beneficial for lowering CO_2 emissions for both B100 and ULSD as pilot fuels.
7. For both B100 and ULSD at 2.5 bar BMEP and maximum PES the BSCO for propane as the primary fuel was much higher than the corresponding methane as a primary fuel value; however, at the same conditions, the THC for propane was considerably lower than the corresponding methane value. A plausible explanation for BSCO and THC trends at these conditions was offered as being due to a competition between fuel (or THC) oxidation vs. CO oxidation. For the B100-propane case, it was hypothesized that owing to the higher reactivity of propane, fuel oxidation would assume importance; while for the methane case, it was hypothesized that CO oxidation would take precedence owing to the slower reactivity of methane.

REFERENCES

1 Yao, M., Zheng, Z., Liu, H., 2009, "Progress and recent trends in homogeneous charge compression ignition (HCCI) engines" *Progress in Energy and Combustion Science,* 35, 398-437, 2009

2 Kokjohn, S.L., Hanson, R.M., Splitter, D.A., Rolf R. D., 2009, "Experiments and Modeling of Dual-Fuel HCCI and PCCI Combustion In-Cylinder Fuel Blending," SAE 2009-01-2647

3 Karim, G. A. 2003 Combustion in Gas Fueled Compression: Ignition Engines of the Dual Fuel Type. Transactions of the ASME: Journal of Engineering for Gas Turbines and Power, Vol. 125, 827-836

4 Karim, G. A. 1987 The dual fuel engine. In *Automotive Engine Alternatives* Ed. R. L. Evans Plenum Press.

5 Gibson, C. M., Polk, A. C., Shoemaker, N. T., Srinivasan, K. K., Krishnan, S. R. 2011 Comparison of Propane and Methane Performance and Emissions in a Turbocharged Direct Injection Dual Fuel Engine. Transaction of the ASME: Journal of Engineering for Gas Turbines and Power, Vol. 133, Issue 9.

6 Papagiannakis, R. G., and Hountalas, D. T., 2003, "Experimental Investigation of Natural Gas Percentage on Performance and Emissions of a D.I. Dual Fuel Engine," Appl. Therm. Eng., 23, pp. 353–365.

7 Daisho, Y., Koseki, T., Saito, T., and Kihara, R., 1995, "Combustion and Exhaust Emissions in a Direct-Injection Diesel Engine Dual-Fueled with Natural Gas," SAE Paper No. 950465

8 Srinivasan, K.K., Krishnan, S.R., Singh, S., Midkiff, K.C., Bell, S.R., Gong, W., Fiveland, S.B., Willi, M., 2006, "The Advanced Low Pilot Ignited Natural Gas Engine-A Combustion Analysis," *Journal of Engineering for Gas Turbines and Power,* Vol. 128, Issue 1., pp. 213-218

9 Krishnan, S.R., Srinivasan, K.K., Singh, S., Bell, S.R., Midkiff, K.C., Gong, W., Fiveland, S.B., Willi, M., 2004, "Strategies for Reduced NOx Emissions in Pilot-

Ignited Natural Gas Engines," *Journal of Engineering for Gas Turbines and Power,* Vol. 126, Issue 3, pp. 665-671

10 Splitter, D., Hanson, R., Kokjohn, S., Reitz, R., 2010 Reactivity Controlled Compression Ignition (RCCI) Heavy-Duty Engine Operation at Mid-and High-Loads with Conventional and Alternative Fuels SAE 2011-01-0363

11 Reed, H.M., Kokjohn, S.L., Splitter, D.A., Reitz, R.D., 2010, "An Experimental Investigation of Fuel Reactivity Controlled PCCI Combustion in a Heavy-Duty Engine" SAE 2010-01-0864

12 Kokjohn, S.L., Hanson, R.M., Splitter, D.A., Rolf R. D., 2009, "Experiments and Modeling of Dual-Fuel HCCI and PCCI Combustion In-Cylinder Fuel Blending," SAE 2009-01-2647

13 Splitter, D., Kokjohn, S., Rein, K., Reed, H., Sanders, S., Reitz, R., 2010, "An Optical Investigation of Ignition Processes in Fuel Reactivity Controlled PCCI Combustion," SAE 2010-01-0345

14 Poonia, M. P., Ramesh, A., and Gaur, R. R., 1999, "Experimental Investigation of the Factors Affecting the Performance of a LPG—Diesel Dual Fuel Engine," SAE Paper No. 1999-01-1123.

15 Stewart, J., Clarke, A., and Chen, R., 2007, "An Experimental Study of the Dual-Fuel Performance of a Small Compression Ignition Diesel Engine Operating With Three Gaseous Fuels," Proc. Inst. Mech. Eng., Part D J. Automob.Eng. 22, 8, pp. 943–956.

16 Liu, Z., and Karim, G. A., 1995, "The Ignition Delay Period in Dual Fuel Engines," SAE Paper No. 950466.

17 Jian, D., Xiaohong, G., Gesheng, L., and Xintang, Z., 2001, "Study on Diesel-LPG Dual Fuel Engines," SAE Paper No. 2001-01-3679.

18 Goto, S., Lee, D., Wakao, Y., Honma, H., Mori, M., Akasaka, Y., Hashimoto, K., Motohashi, M., and Konno, M. 1999, "Development of an LPG DI Diesel Engine Using Cetane Number Enhancing Additives," SAE 1999-01-3602

19 Ogawa, H., Miyamoto, N., Li, C., Nakazawa, S, and Akao, K. 2001, "Low Emission and Knock-Free Combustion with Rich and Lean Biform Mixture in a Dual-Fuel IC Engine with Induced LPG as the Main Fuel," SAE 2001-01-3502

20 Yao, M., Zheng, Z., Qin, J. 2006, "Experimental Study on Homogeneous Charge Compression Ignition Combustion with Fuel of Dimethyl Ether and Natural Gas," *Journal of Engineering for Gas Turbines and Power*, Vol. 128, pp.414-420

21 Ogawa, H., Miyamoto, N., Li, C., Nakazawa, S, and Akao, K. 2001, “Smokeless and Low NOx Combustion in a Dual-Fuel Diesel Engine with Induced Natural Gas as the Main Fuel,” Paper No. 3-06, “Proceedings of the Fifth International Symposium on Diagnostics and Modeling of Combustion in Internal Combustion Engines (COMODIA 2001), July 1-4 2001, Nagoya, Japan

22 Nazar, J., Ramesh, A., Nagalingam, B., 2006, “Studies on Dual Fuel Operation of Karanja Oil and Its Bio-Diesel with LPG as the Inducted Fuel,” SAE 2006-01-0237

23 Lapuerta, M., Armas, O., Rodriguez-Fernandez, J., 2008, “Effect of biodiesel fuels on diesel engine emissions,” Progress in Energy and Combustion Science, 34, 198-223, 2008

24 Sun, J., Canton, J.A., Jacobs, T.J., 2010, “Oxides of nitrogen emissions from biodiesel-fuelled diesel engines,” Progress in Energy and Combustion Science, 36, 677-695, 2010

25 SAE International, 2002, "Diesel Engine Emission Measurement Procedure: Recommended Practice," SAE Paper No. J1003

26 Heywood, J.B., 1998, “Internal Combustion Engine Fundamentals,” McGraw Hill, Inc.

27 Kubesh, J.T., 2002, "Uncertainty in the Determination of Thermal Efficiency in Natural Gas Engines," Design, Application, Performance and Emissions of Modern Internal Combustion Engine Systems and Components, ASME, New York, Vol. 39.

28 Yap, D., Megaritis, A., Peucheret, S., Wyszynski, M.W., Xu, H., "Effect of Hydrogen Addition on Natural Gas HCCI Combustion," SAE 2004-01-1972

29 Kalghatgi, G.T., Head, R.A., "Combustion Limits and Efficiency in a Homogeneous Charge Compression Ignition Engine," Intl. J. Eng. Res. Vol. 7, pp. 215-236, 2005

30 Peters, N., 1999, “The Turbulent Burning Velocity for Large-Scale and Small-Scale Turbulence,” J. Fluid Mech., 384, pp. 107–132.

31 Mueller, C., Boehman, A. L., Martin, G. C. 2009, “An Experimental Investigation of the Origin of Increased NOx Emissions When Fueling a Heavy-Duty Compression-Ignition Engine with Soy Biodiesel,” SAE 2009-01-1792

32 Sjoberg, M. and Dec, J., “An Investigation into Lowest Acceptable Combustion Temperatures for Hydrocarbon Fuels in HCCI Engines” Proc. Of Comb. Inst, 30 (2), pp. 719-726

APPENDIX A

AIR-FUEL STOICHIOMETRIC AND MOLE FRACTION CALCULATIONS

Objective I: To calculate the Air-Fuel stoichiometry for pilot fuel (biodiesel or ultra-low sulfur diesel) and primary gaseous fuel such as methane, propane, natural gas.

We assume that the pilot fuel is represented by $C_XH_YO_Z$ and the primary gaseous fuel is represented by C_AH_B. The chemical stoichiometric equation for complete combustion of the two fuels, i.e., $C_XH_YO_Z$ and C_AH_B is given by equation A.1.

$$kC_XH_YO_Z + (1-k)C_AH_B + A_S(O_2 + 3.76N_2) \rightarrow n_1CO_2 + n_2H_2O + n_3N_2 \quad \text{(A.1)}$$

Where, k is the mole fraction of pilot fuel and 1-k is the mole fraction of the primary gaseous fuel in the biodiesel-primary gaseous fuel mixture.

Carbon, Hydrogen and Oxygen balances are performed to yield the following:

Carbon balance :

$$kX + (1-k)A = n_1 \quad \text{(A.2)}$$

Hydrogen balance :

$$kY + (1-k)B = 2n_2 \quad \text{(A.3)}$$

Oxygen balance :

$$kZ + 2A_S = 2n_1 + n_2 \quad \text{(A.4)}$$

Solving for A_s

$$A_S = k\left(X + Y/4 - Z/2\right) + (1-k)\left(A + B/4\right) \quad \text{(A.5)}$$

From this the mass-based air-fuel stoichiometric ratio is determined as:

$$AF_{st-tot} = \frac{A_S MW_{air}}{kMW_l + (1-k)MW_g} \quad \text{(A.6)}$$

Where, MW_{air} is the molecular mass of air and MW_l and MW_g are the molecular masses of pilot fuel and primary gaseous fuel, respectively.

In equations A.2-A.6, the value of k is still unknown; however, this can readily be obtained from the mass flow rates of pilot fuel and primary gaseous fuels, and the formula for percentage energy substitution (PES). This is demonstrated in equations A.7-A.8 below.

Objective II: To determine the mole fractions of pilot fuel and primary gaseous fuel from PES.

We know from Eq. 2.2 in the manuscript that the percentage energy substitution or PES is given by:

$$PES = \frac{\dot{m}_g LHV_g}{\dot{m}_l LHV_l + \dot{m}_g LHV_g} \times 100\% \tag{A.7}$$

$$PES = \frac{(1-k) MW_g LHV_g}{k MW_l LHV_l + (1-k) MW_g LHV_g} \times 100\% \tag{A.8}$$

Since the mass flow rates of the pilot fuel and primary gaseous fuel, and their respective lower heating values are either measured or known apriori, the percentage energy substitution is calculated using equation A.7. Once the PES is known, then the mole fractions of biodiesel and the primary gaseous fuel can be determined from equation A.8, and the air-fuel stoichiometric ratio can be calculated using equation A.6.